A SIMULATION MODEL OF INDOOR ENVIRONMENTS FOR ULTRASONIC SENSORS

A THESIS

SUBMITTED TO THE DEPARTMENT OF ELECTRICAL AND

ELECTRONICS ENGINEERING

AND THE INSTITUTE OF ENGINEERING AND SCIENCE

OF BILKENT UNIVERSITY

IN PARTIAL FULFILLMENT OF THE REQUIREMENTS

FOR THE DEGREE OF

MASTER OF SCIENCE

by

Ali Bilgin

August 2003

I certify that I have read this thesis and that in my opinion it is fully adequate, in scope and in quality, as a thesis for the degree of Master of Science.

Prof. Dr. Billur Barshan (Supervisor)

I certify that I have read this thesis and that in my opinion it is fully adequate, in scope and in quality, as a thesis for the degree of Master of Science.

Prof. Dr. Enis Çetin

I certify that I have read this thesis and that in my opinion it is fully adequate, in scope and in quality, as a thesis for the degree of Master of Science.

Prof. Dr. Ayhan Altıntaş

Approved for the Institute of Engineering and Science:

Prof. Dr. Mehmet B. Baray
Director of the Institute Engineering and Science

ABSTRACT

A SIMULATION MODEL OF INDOOR ENVIRONMENTS FOR ULTRASONIC SENSORS

Ali Bilgin
M.S. in Electrical and Electronics Engineering
Supervisor: Prof. Dr. Billur Barshan
August 2003

This thesis addresses the problem of extracting the map of an unknown environment from echo signals received by ultrasonic transducers. A new map-building method is developed and demonstrated through simulations for ultrasonic sensors. Ultrasonic transducer arrays are used for scanning the environment. The method uses ultrasonic range and amplitude data to build a two-dimensional map of an unknown environment. All of the amplitude information is taken into account in the simulation studies. The received echo amplitude where it exceeds a predefined threshold is used for drawing the map. The method can extract the surface profiles from the received echoes with knowledge of transducers' position. With this method, sonar signal returns from arbitrary indoor environments can be represented realistically and with relatively low computation time. Different types of environments composed of planar surfaces, corners, edges, cylinders, and arbitrarily curved surfaces have been considered. An error criterion is developed to assess the accuracy of the extracted maps. Randomly located and randomly oriented configuration of transducers gives the best estimate of the surface profiles. Most of the closed room models is a continuous combination of basic shapes. The wall-following algorithm is employed to extract the profiles of indoor environments. The results indicate that many of the indoor environment profiles can be accurately extracted by this method. The method is fast and suitable for real-time map building applications.

Keywords: Sonar sensing, range sensing, distance measurement, surface profile extraction, map building, position estimation.

ÖZET

ULTRASONİK ALGILAYICILAR İÇİN İÇ MEKANLARIN BENZETİM MODELİ

Ali Bilgin
Elektrik ve Elektronik Mühendisliği, Yüksek Lisans
Tez Yöneticisi: Prof. Dr. Billur Barshan
Ağustos 2003

Bu tezde ultrasonik dönüştürücülerce alınan yankı işaretlerinden bilinmeyen bir ortamın haritasının çıkarım problemi ele alınmıştır. Yeni bir harita çıkarım yöntemi geliştirildi ve yöntem ultrasonik algılayıcılar için benzetimler yoluyla kanıtlanmıştır. Ultrasonik dönüştürücü dizileri ortam taraması için kullanıldı. Yöntem, bilinmeyen bir ortamın iki boyutlu haritasını çıkarmak için ultrasonik erim ve genlik verisini kullanıyor. Tüm genlik bilgisi benzetim çalışmalarında hesaba katılmıştır. Alınan yankının genliğinin önceden tanımlanan eşik değerini geçtiği yerler kestirim haritasının çizilmesinde kullanılmıştır. Yöntem, yüzey profillerini alınan yankılardan yüzey profillerini dönüştürücülerin konumlandırılması bilgisiyle çıkartabilmektedir. Bu yöntemle iç mekan ortamlarından geri dönen sonar işaretleri gerçekçi olarak gösterilebilir. Düzlemler, köşeler, kenarlar, silindirler ve rasgele eğimli yüzeylerden oluşan değişik tiplerde ortamlar göz önüne alınmıştır. Çıkarılan haritaların doğruluğunu belirlemek için bir hata kriteri geliştirildi. Dönüştürücülerin rasgele yerleştirilmiş ve gelişi güzel yönlendirilmiş biçimi, yüzey profillerinin en iyi tahminini vermektedir. Kapalı oda modellerinin çoğu temel şekillerin dairesel olarak kesintisiz yerleştirilmiş bileşiminden oluşmaktadır. Duvar takibi algoritması ile de iç mekanların haritaları elde edildi. Sonuçlar göstermektedir ki iç mekan profillerinin çoğu bu yöntemle tam olarak kestirilebilmektedir. Yöntem hızlıdır ve gerçek zamanlı harita çıkarımı uygulamaları için uygundur.

Anahtar sözcükler: Sonarla algılama, uzaklık algılama, uzaklık ölçümü, yüzey profili çıkartılması, harita çıkarımı, konum kestirimi.

Acknowledgement

I would like to express my gratitude to my supervisor Prof. Dr. Billur Barshan for her instructive comments in the supervision of the thesis.

I would like to express my special thanks and gratitude to Prof. Dr. Enis Çetin and Prof. Dr. Ayhan Altıntaş for showing keen interest in the subject matter and accepting to read and review the thesis.

Contents

List of Figures

This work is dedicated to my wife,

who always gives me love and support.

Chapter 1

Introduction

1.1 Motivation

Identification of environments is an important problem for robot localization and navigation. Many different methods and different kinds of sensors can be used for defining a robot's surroundings. Ultrasonic sensors, lasers, infrared sensor and cameras are widely used for classification of objects in indoor environments. Infrared sensors can be used for relatively short distance measurements. Laser and camera-based systems require complex mathematics and high cost. Today, ultrasonic sensors are mostly used for environment identification because of their low cost and calculation simplicity. The basic problem with ultrasonic sensor identification systems is the resolution of the estimated map. Low resolution maps can be formed with shorter computation time, but most of the objects cannot be extracted from the map. High resolution maps require very long computation time and much memory. New methods must be found for identification of objects from high resolution maps with shorter computation times and cheaper sensors. The proposed method is a solution for low cost and fast map building.

1.2 Literature Review on Map Building

The aim of this work is to extract the profiles of indoor environments using ultrasonic sensors. Physical models of ultrasonic sensors are developed and implemented for object classification and position estimation. Kuc and Siegel [29] developed mathematical models for the echo signals from plane, corner, and edge. Time-of-flight (ToF) information is used for the mathematical representation of the echo. In a typical indoor environment, there are many different types of objects with varying surface curvature. Some objects have basic shapes such as planes, corners, edges, and cylinders. Most surfaces have complex surface profiles which are combination of these basic shapes. In the ultrasonic sensing process, the echo signals are also contaminated with noise.

Researchers have employed different map-building techniques. Mostly used map building techniques are landmark-based, feature-based, and grid-based techniques. In these works, ultrasonic, infrared sensors, and cameras mounted on mobile robots are used for scanning the environment. Mostly, Extended Kalman Filter (EKF) is used for robot localization and feature-based map building. In this work, properties of ultrasonic sensors are simulated with accurate sensor localization.

Hu and Gu used laser scanners for landmark position estimation and robot localization in manufacturing industry [13]. Their system updates landmarks in a dynamic environment. A solution to the simultaneous map building and localization problem is given by Dissanayake [25]. A radar mounted vehicle is used for outdoor environments. Laser reflectors are used as landmarks. When a new landmark is detected, landmark-map is updated. EKF is used for vehicle localization and map building. Cetto and Sanfeliu used landmark-based mapping techniques using cameras [2]. They defined detected landmarks as a state. When new sensor information comes, data is compared to see whether it will fall within the field of view. If it is within the field of view, then landmark map state is updated. In another work, they put landmark map features into map state vector and try to estimate surface profile of a concurrent map [3]. When a new landmark is detected, map feature covariance matrix is updated. Determinant of

the map covariance matrix decreases at each landmark detection. Guivant and Nebot give a new method for scanning large areas [17]. They used landmarks for map building, but Compressed Extended Kalman Filter is used for localization of the robot. This filter reduces memory requirements with respect to EKF, and enables scanning of large areas. Betke and Gurvits proposed a new algorithm for map building [21]. They represent landmarks by complex numbers. The algorithm they propose runs in time linear in the number of landmarks, and provides estimations very close to the actual robot position. Sempé used a region-based map building technique [11]. Lines are used for determining regions. Markov localization is used for robot position estimation. Castellanos and Tardos used multisensor information coming from a laser and a camera for scanning the environment [15]. The environment is represented with landmarks based on topologic relations between sensor data. Arras used probabilistic feature-based mapping and robot localization [20]. In another work, Arras used segmentation for classifying objects [19]. Kam and Zhu use infrared and ultrasonic sensors for scanning the environment [24]. Features are extracted as a result of sensor fusion. The feature map is generated and localization of the robot is done using EKF. Newman describes a method which enables a robot using feature-based navigation techniques to explore its environment [27]. Baltzakis propose a mapping algorithm that utilizes features in order to produce maps suitable for continuous-state localization algorithms [12]. Jensfelt use condensation with planned sampling as a tool for doing feature-based global localization in a large and semi-structured environment [26]. Guivant defines features as state vectors [18]. At each scan, states are updated. Wullschleger uses segment-based mapping [10]. Features are updated by determining weighted averages of segment lines. Jeon and Kim present a feature-based probabilistic map building algorithm [14]. Their proposed algorithm uses ToF and amplitude information in indoor environments. At each scan, received data is compared with previous data. Prediction of the estimation is done for all types of previously detected known targets.

Another class of approaches for map-building employs grid-based techniques. Elfes gives the basics of grid-based mapping [1]. Their proposed system uses sonar range data to build a multilevel description of the robot's surroundings.

Sonar range readings are classified using probability profiles as empty and occupied areas. Elfes defined occupancy map as unknown, empty and occupied areas. Schiele and Crowley modelled the environment based on two certainty grids [4]. Local and global models are used for robot and environment position estimations. Varveropoulos represented the global map as an occupancy grid [30]. At each new range measurement, an occupancy value and a certainty value is stored in the map. Final map is drawn with respect to occupancy and certainty values in gray-scale image. Murray and Jennings used stereo vision techniques for map building [8]. Each grid is assigned a value which represents the probability that it is occupied. Initially, the environment is unknown and grids are assigned a probability of 0.5 of being occupied. Each grid value is incremented or decremented with respect to the scanned area. Final map is displayed with grid values between 0 to 255. In another work, Jennings and Murray used two robots which navigate and explore their environment [5]. Grid-based stereo vision map building is used for mapping. Borenstein and Koren used ultrasonic sensors for scanning [16]. They defined map with respect to sensors' range readings. Occupancy probability grid values are incremented. Then, sonar is moved for scanning another area. In the histogram map, empty grid values are decremented and occupancy grid areas are incremented. They used grow-rate operator to find the final grid-map. Novick and Crane represented grids as occupancy probabilities [9]. They proposed a method which uses the physical properties to determine grids for updating and used fuzzy modelling of sensor's uncertainty to actually update the grid-cell using a nonhomogeneous Markov chain.

Caccia gives a new mapping approach with two sonar heads [22]. Sonar readings from two sonar heads are located on the grid map. Yi and Khing used Dempster-Shafer's evidence method to make grid-based occupancy map [31]. They reduced false readings in ultrasonic responses corrupted by specular reflections from confined environments. Jun gives a new method for occupancy grid-maps [23]. Occupancy values are determined based on sensor readings and by applying the conditional probability of occupancy using Bayes' rule. The probability map is updated using sensor information and a priori statistics of the dynamic environment.

In this work, a new method which finds a solution to the inverse problem of curvature estimation is presented. Başkent and Barshan [6, 7] used morphological processing techniques to determine surface profiles using ToF information. They located transducers randomly in the scanning area. For the same sensor transmitting and receiving, the reflecting point is presented to be on a circular arc within the transducer sensitivity region. They used an elliptical arc if the transmitting-receiving transducers are different. Thinning, pruning and curve fitting techniques were used to produce the final surface profile estimate.

Here, an alternative approach is developed for the inverse problem of surface profile estimation. Both amplitude and ToF information is taken into account and more information about surface coming from neighboring transducers is employed. Different types of surfaces can be scanned and the surface profile estimate can be drawn with a few mathematical operations. Spatial low-pass filtering and thinning is used for drawing the map. Curve-fitting techniques are used to complete the surface profile estimation.

1.3 Organization of the Thesis

This thesis is organized as follows: In Chapter 2, basics of sonar sensors are given. Properties and working principle of the simulated Polaroid 6500 series ultrasonic sensor is explained. Chapter 2 also includes the proposed simulation method for estimating surface profiles of basic objects. An extended version of the algorithm is also given for building maps of indoor environments. In Chapter 3, simulation results are presented. Results for planes, corners, edges, cylinders, and sinusoidal surfaces are given for the measurements from short, medium, and far distances from the actual surface profile. In this chapter, closed room simulation results are also presented. Finally, Chapter 4 draws some conclusions and indicates some directions for future research.

Chapter 2

Basics of Sonar Sensors

Operating frequencies of ultrasonic transducers vary between 40-250 kHz. As the resonance frequency of the ultrasonic sensor increases, attenuation in the air increases as well. Due to this fact, low resonance frequency ultrasonic transducers are widely used in robotics applications. Speed of sound in air is changes with both temperature and humidity. Speed of an ultrasonic signal as a function of temperature in air is represented as:

$$c = 331.4\sqrt{\frac{T}{273}} \tag{2.1}$$

At room temperature, the speed of the ultrasonic wave is about 343.3 m/sec. Another factor which effects the performance of an ultrasonic transducer is its beamwidth. A transducer with wide beamwidth can detect unwanted signals. On the other hand, it has more coverage. The half beamwidth angle of the transducer is given by:

$$\theta_0 = \sin^{-1}\left(\frac{0.61\lambda}{a}\right) \tag{2.2}$$

where a is the radius of the transducer and λ is the wavelength at the resonance frequency.

In this study, the Polaroid 6500 series ultrasonic sensor is employed which is the most commonly used ultrasonic transducer in indoor mobile robotics applications. It has a resonance frequency of 50 kHz. The radiation pattern of this

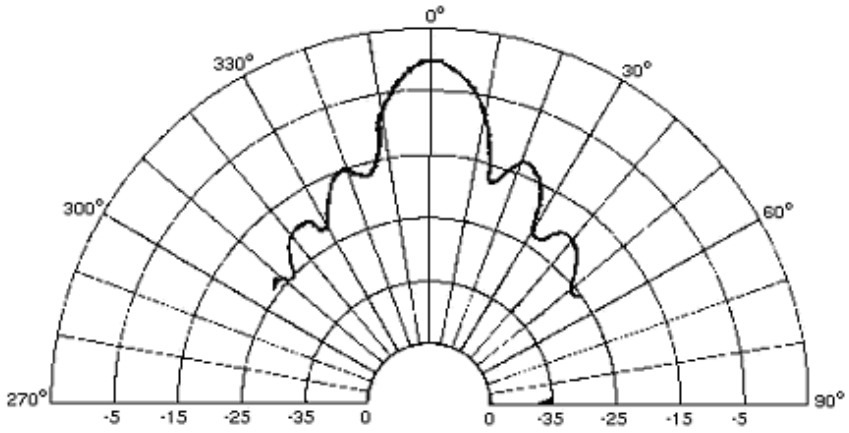

Figure 2.1: Polaroid 6500 series radiation pattern. Resonance frequency: 50 kHz (Polaroid 1987).

transducer is illustrated in Figure 2.1. The amplitude of the signal can also be measured. Polaroid transducers can measure the distance up to about 10 m with an accuracy decreasing with angular deviation from the LoS and with distance from the surface of the transducer. When both time and amplitude information is used, it is possible to classify objects and to estimate their positions.

The signal emitted by the Polaroid transducer is modelled as a sinusoid with Gaussian envelope. The echo reflected from surfaces is detected by the transducer. The echo signal is modelled as a delayed transmitted pulse with additive noise. Time delay between the transmitted signal and received echo is the time-of-flight (ToF). When this information is multiplied with the speed of the wave, the wave's round-trip travel distance can be easily calculated from $r = ct_o$. For planar surfaces, the echo can be represented as a signal transmitted from a virtual transducer which is away from the real transducer by the round-trip distance (Figure 2.2).

Ultrasonic transducers can be configured as arrays. The reason for array usage is to improve the resolution and the accuracy of position estimation. In transducer arrays, one of the transducers can be activated for transmitting ultrasonic waves and one, some, or all of the transducers can be activated for receiving the echoes.

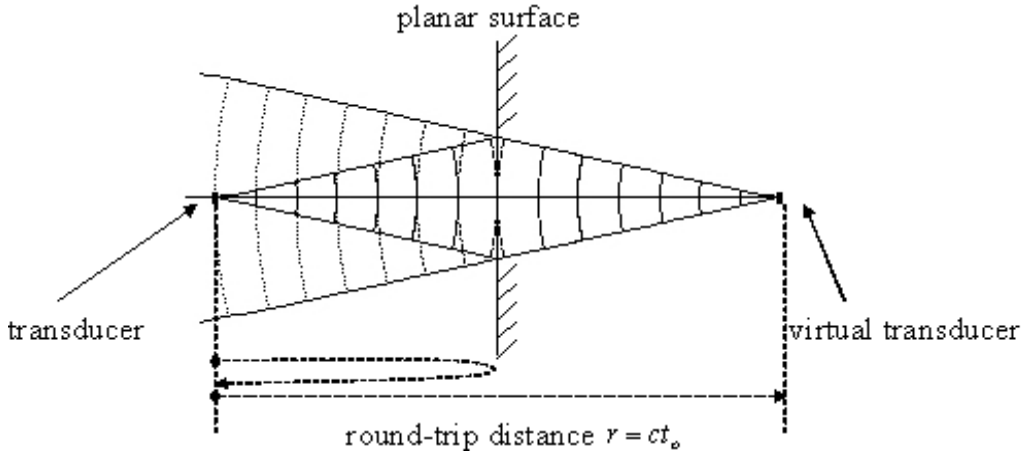

Figure 2.2: Calculation of round-trip distance for a planar surface. The echo is modelled as if it is transmitted from the virtual transducer.

All possible combinations of transmitter-receiver pairs can be used. With the help of echoes arising from other transducers, we can have better information about the position and type of the reflecting object.

2.1 The Simulation Model

In the simulation studies, a 10mx10m closed environment is used. The environment is divided into 1000x1000 intervals and represented with 1000x1000 pixels so each pixel corresponds to a $1cm^2$ area which is called a cell. In the simulations, these cells have default background color white. Cells are filled with black color if they are occupied.

Simulations are carried out in MATLAB 6.0.0.88 (R12) on a Pentium-III 733MHz CPU and 384MB SDRAM PC with Windows XP operating system. Beamwidth of the Polaroid transducer is taken as 24° with half beamwidth angle θ_0=12°. The line-of-sight (LoS) and the sensitivity region of this simulated transducer is illustrated in Figure 2.3.

The transmitted signal is modelled as a sinusoidal signal with shifted Gaussian

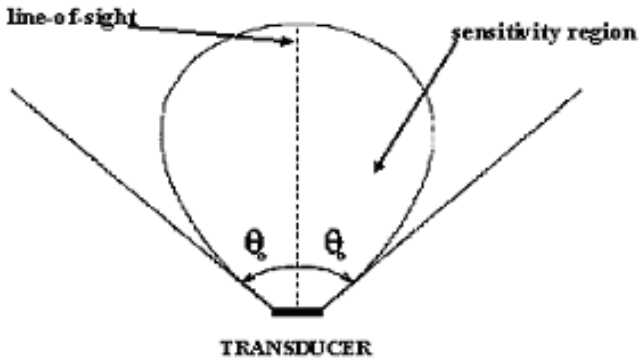

Figure 2.3: The sensitivity region of an ultrasonic transducer. The transducer can both transmit and receive ultrasonic waves.

envelope (Figure 2.4). The maximum amplitude of the transmitted signal is 5 units. Mathematical representation is given by:

$$p(t) = \begin{cases} K \exp(\frac{-(t-3\sigma)^2}{2\sigma^2}) \sin(2\pi f_r t) & , 0 \leq t \leq 6\sigma \\ 0 & , \text{otherwise} \end{cases} \tag{2.3}$$

where K is a normalization multiplier. In the simulation process, zero-mean Gaussian noise with standard deviation varying between 0.5 and 1.5 units is added to the received signal to realize different noise levels.

The actual surface profiles are drawn in two-dimensional space. First, a transducer array with 10 transducers is formed. The first element of the array is randomly located in the environment. Other elements are located one by one with different separations. For new array localization, the first element of the array is located away from last element of the previous array with a randomly generated distance. In the transducer localization process, if one of the elements is located near the boundary of the surface, the localization process is terminated and simulation is done with the presently located transducers. The length of separations between the centers of the transducers varies between 5 cm and 11 cm. The diameter of the transducer is 4 cm and represented with 4 pixels and their orientations are randomly generated between 0° and 180°. Separations of the centers of the transducer arrays vary between 50 cm and 165 cm. In the model,

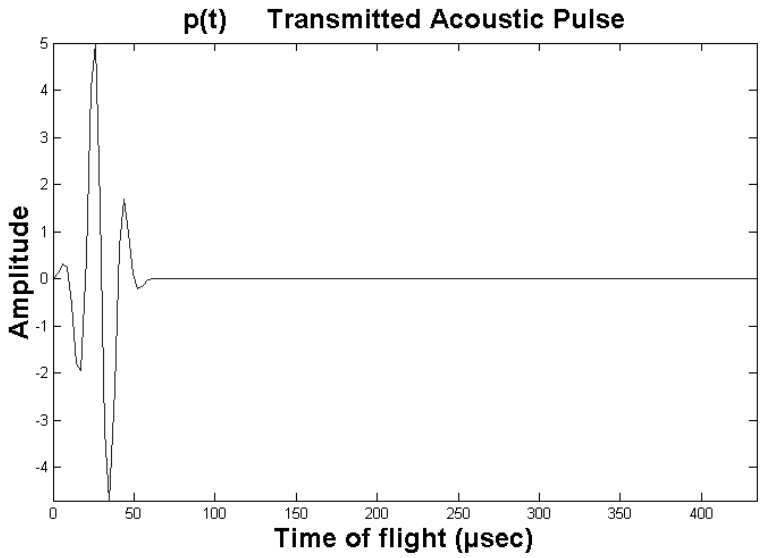

Figure 2.4: The transmitted signal.

the sensitivity regions of transducers are divided into 25 parts starting at -12° and ending at $+12^\circ$.

2.1.1 The Simulation Model for Basic Target Shapes

The simulation studies are divided into five parts. The first and second parts are for generating the transmitted signals. The third and fourth parts are for drawing the two-dimensional map of the environment. Filtering and error calculations are performed in the fifth part.

In the first part, only the signals reflected from the LoS are used for target type and location estimation. In this case, only the echoes arising from the transmitting transducer are taken into account in constructing the received signal. The echoes coming from orientations within $\pm 1^\circ$ of the transducer normal are taken as the LoS return signals. For the LoS reflected signals, the distances are calculated with the help of ToF information and the velocity of the ultrasonic wave in air. Transmitting and receiving transducer indices and ToF information are stored in an array.

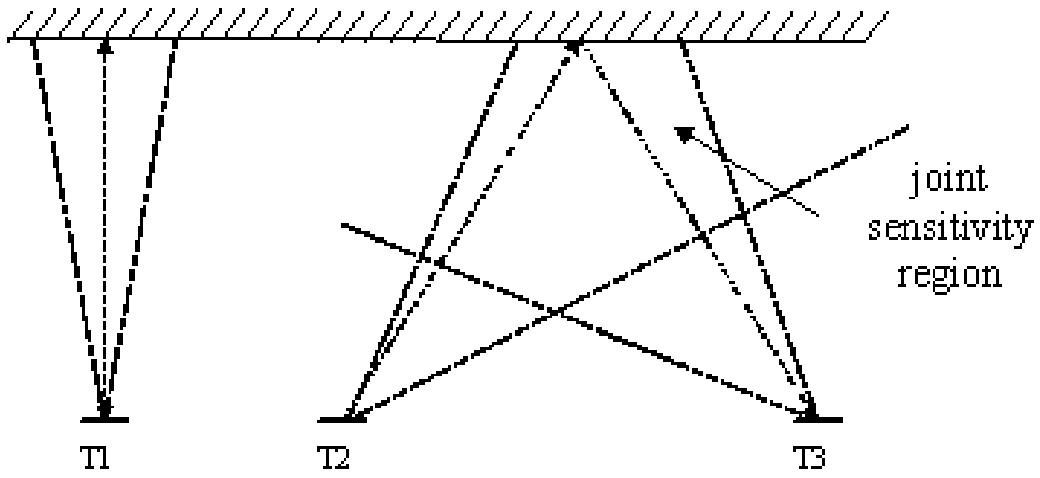

Figure 2.5: On the left, we illustrate the same transducer (T1) transmitting and receiving. On the right, T2 transmits and T3 receives.

In the second part of the simulations, all the elements of the transducer array are used. The transducers are activated one at a time. Transmitting and receiving transducer pairs are determined (Figure 2.5). The echoes obtained with all of the transducers are calculated. Transmitting and receiving transducer pairs and ToF of the echo signal are stored in an array. Finally, at the generating stage, LoS reflected signals and transmitting-receiving transducers pair signals are summed with required time delays which come from ToF information and zero-mean Gaussian noise is added to each of the received signals.

The third and the fourth parts of the simulations address the problem of extracting the surface profile from the received echoes. In most of the echo calculations, the point where the received signal exceeds a preset threshold gives the LoS round-trip distance. The received signal is compared with the threshold level which is set equal to 4 units. The noise standard deviation varies between 0.1 and 1.2 units and the maximum amplitude of the transmitted signal is 5 units. The first point where the received signal exceeds the threshold is taken as the LoS return signal and a 24° arc is drawn from the center of the transducer with a radius equal to half of the round-trip distance.

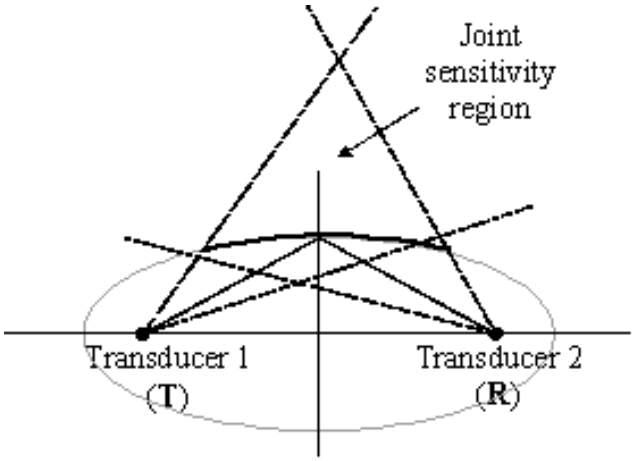

Figure 2.6: Transducers located at the foci of the ellipse.

Then, the fourth stage of the simulations begins. Other points where the received echoes exceed the threshold are taken into account. At each point, the ToF is calculated. Given a transmitting transducer (T) and a receiving transducer (R), the locus of points which corresponds to a constant ToF value is an ellipse with foci located at T and R. In other words, the reflection point could be located anywhere on the ellipse. When a signal is transmitted from a transducer which is located at one of the foci of the ellipse, and the reflected signal is received at the other transducer located at the other focus, the echo must be reflected from a point on the elliptical arc contained within the joint sensitivity region. With this information and the two-dimensional array which was calculated in part two, ellipses are drawn such that transmitting and receiving transducers are located at the two foci of the ellipses. With the ToF information, distance-of-flights are calculated. Major axes of the ellipses are taken as half the distance-of-flights. As a final stage, the elliptical arc which falls within the joint sensitivity region of a given transmitter-receiver pair is drawn (Figure 2.6).

In the fifth stage of the simulations, spatial low-pass filtering is applied to the two-dimensional map obtained at the previous stages [28].

The convolution matrix for the filter is given as:

$$\frac{1}{9} \times \begin{bmatrix} 1 & 1 & 1 \\ 1 & 1 & 1 \\ 1 & 1 & 1 \end{bmatrix} \tag{2.4}$$

After filtering the process map, a lot of redundant lines occur. Thinning process [28] is applied to the filtered map. Each pixel of the map is compared with the matrix defined as:

$$\begin{bmatrix} 0 & 0 & 0 \\ X & 1 & X \\ 1 & 1 & 1 \end{bmatrix} \tag{2.5}$$

where X's denote don't care condition. The pixels which match with the matrix conditions are preserved and others are zeroed.

The simulation model works based on randomly localized transducers and noisy environment conditions. Because of these factors, some parts of the surface profile may not be detected and there may be gaps on the estimated surface profiles. Polynomial fitting techniques are applied for completing the estimated map. As a final process, the estimated surface profile is compared with the actual surface profile and the root-mean-square (RMS) error, defined by the following equation, is calculated.

$$E_{rms} = \sqrt{\frac{1}{N} \sum_{i=1}^{N} \left| C_{actual}\left(x_i\right) - C_{estimated}\left(x_i\right) \right|^2} \tag{2.6}$$

The Matlab program uses a large number of matrix operations and arrays, so some memory problems may occur. At the beginning of the programming stage, received signals with all possible transmitter-receiver combinations are calculated. 100 transducers are randomly located across from the 10 m wall. For calculating one transducer's received echo, we need to check if any surfaces are detected with its joint sensitivity region with other transducers. This process increases computation time up to several minutes to scan 10 m length surface, which is not suitable for real-time applications. Drawing one wall map of 10 m room with 100 transducers has 100! computation stages. Performance of this method was

not so good. When a 10 m surface is divided into 1 m parts and when the parts are scanned with randomly located and oriented transducers, the computation cycle reduces to 10 times 10!, resulting in a surface profile with better resolution. Surface scanning time of the 10 m long surface reduces to approximately 1 minute. Most of this time is spent for matrix operations. Less than half of this time is spent for drawing the surface features obtained. In real time, the signal can be detected by the transducers in a few microseconds. The points where the signal exceeds the threshold level are taken into account. ToF values are calculated and ellipses are drawn with the help of two-dimensional array which contains information on transmitter/receiver transducer pairs. Calculating and drawing the surface estimate takes less than half a minute for a 10 m surface.

2.1.2 The Wall-Following Algorithm

In the simulation of a closed environment, the algorithm scans each wall of a closed area, and then combines these results and produces the final estimated map. For edges, corners, and cylinders multiple reflections occur. Multiply-reflected echoes attenuate and may stay below the threshold. Walls of corners and edges can be detected if they are within the sensitivity region. The algorithm locates array elements on the same line and only a small fraction of the scanning area can be detected. Forward and backward directions of the transducer array cannot be detected so that one of the walls of edges and corners can be detected. An extended version of the algorithm must be developed for scanning edges, and corners, and obtaining a higher resolution map. Circularly located transducers can scan all of the environment without dividing the environment map into parts. Especially for edges and corners, circular transducer array can follow the surface profile of these objects and extract their surface profiles with both walls and vertices.

In the wall-following algorithm, eight transducers are used for scanning the environment. Transducers are oriented with 45° intervals starting at 0° and ending at 315° around a circle of radius 6.5 cm. This circularly located array can move up and down or right and left. The center of this array is randomly

localized in the room and the positions of the transducers are stored in a map. All of the eight transducers are activated for scanning. Transducers' LoS lines are drawn in the estimated map and also elliptical arcs are drawn in the quarter of the LoS distance from the centers of the transducers. After scanning at the first position, the center of the array is moved by one step size which is the shifting size of the center of the array in the 2-D map in clockwise or counterclockwise directions. Moving direction is determined by comparing the vertical and horizontal distances on the base frame of the array. Starting point and direction is stored and direction is changed when the shortest distance is along the moving direction. This procedure goes on until transducer array approaches the starting point. When the transducer array comes to a position which is signed in the transducer map, the program is terminated.

Chapter 3

Simulation Results

In the simulations, four different kinds of surface profiles are used. Basic types of surface profiles are illustrated in Figure 3.1. Plane, corner, edge, cylinder, and sinusoidal surface profiles are used in the simulations and the results are presented in Figures 3.1-3.18. In the first planar surface model, a wall is located 9 m away from origin of the environment along the x direction, (Figure 3.1(a)). In the second model, a corner model is illustrated in Figure 3.1(b). Vertex of the corner is located 10 m away from the origin of the environment map along the x direction. For the third model, an edge is used and the vertex of the edge is located 6.5 m away from the origin along the x direction (Figure 3.1(c)). In Figure 3.1(d), a cylinder with radius 2 m located in the scanning area. In Figure 3.1(e) a first-order sinusoidal surface is located 8 m away from the origin of the environment along the x direction. Finally, a closed room model is used for map building (Figure 3.1(f)).

Simulation program is run with different transducer and actual surface distances. In short distance simulations, distance between the transducer array and the surface is taken as 1.5-2 m. For medium distance simulations, it is taken 3-5 m and for far distance simulations it is taken as 7-9 m.

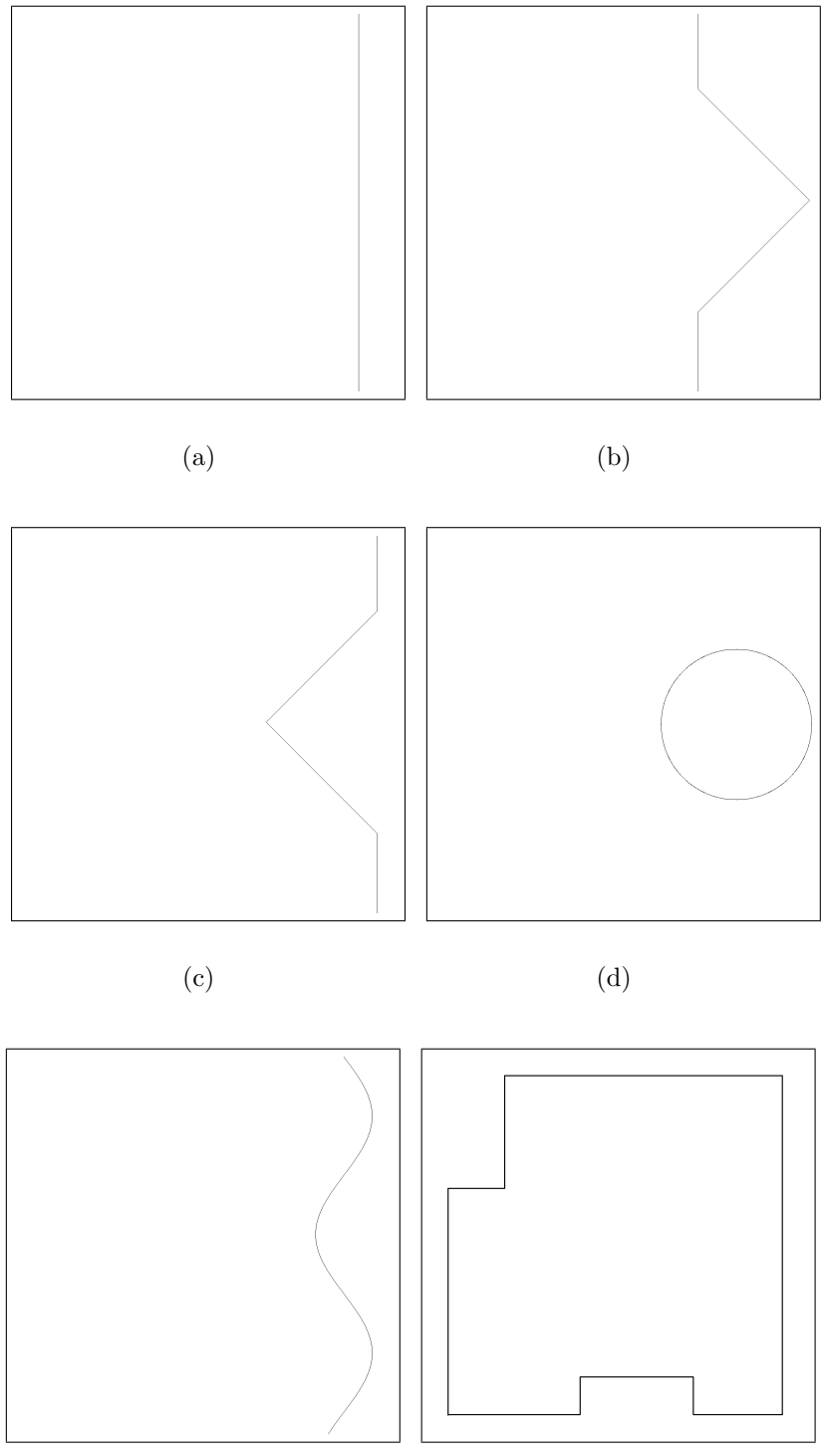

(a) (b)

(c) (d)

(e) (f)

Figure 3.1: Surfaces modelled; a) plane, b) corner, c) edge, d) cylinder, e) sinusoidal surface, and f) closed environment.

3.1 Results for the Plane

In the simulation model of planar surfaces, an array with 10 transducers is used. The first element of the transducer array is randomly located in the environment. Other elements of the array are located away from the first element. Separations between centers of the elements of the array vary between 5 to 12 cm. Addition of the array elements continues until total array length reaches 10 m. In the first run of the simulation program, array elements are localized 7 m away from the wall. The distance between the actual surface profile and the transducers is 2 m (Figure 3.2(a)). The estimation result for the planar surface is presented in Figure 3.2(a). Simulation result without filtering is presented in Figure 3.2(b). A spatial low-pass-filter (LPF) is applied on the estimated surface profile. Some of the unscanned surface profile is estimated (Figure 3.2(c)). This procedure also increases redundant arcs. Thinning process is applied for clearing redundant arcs (Figure 3.2(d)). A polynomial fitting procedure is applied for finalizing the estimation of the surface profile (Figure 3.2(e)). RMS error for the first run is 0.72 cm.

After the first run, the simulation program is re-run for the conditions in which array elements are localized 4 m away from the surface of the planar wall (Figure 3.3(a)). Results of the simulation stages 1-4 are presented in Figure 3.3(b). This result is convolved with a LPF and then, the thinning procedure is applied (Figure 3.3(c)- 3.3(d)). Final estimation result with polynomial fit of order 7 is presented in Figure 3.3(e) with an RMS error of 3.14 cm.

For the third run of the simulation, array elements are localized 8 m away from the exact surface profile (Figure 3.4(a)). Result of the first four stages of the simulation is presented in Figure 3.4(b). In Figure 3.4(c), filtered map and in Figure 3.4(d) thinned result are shown. Final estimated result is shown in Figure 3.4(e)with an RMS error of 6.69 cm.

In the simulation studies, the RMS error is calculated with respect to the LoS distance from the actual surface profile. In the calculation of the RMS error, LoS distances are taken starting from 2 m ending at 8 m. For each LoS distance,

simulation is run five times. Averages of the RMS error for these simulations are displayed in Figure 3.5. RMS error is proportional to the LoS distance. As the position of the array elements move away from the surface profile, the RMS error increases. For large distances between the transducer array and actual surface profile, number of gaps on the estimated surface profile increases. In the polynomial fitting process, these gaps increase the RMS error. All of the RMS calculations are done for the simulations with no noise.

In the simulations, RMS error is calculated for varying noise levels. Simulation for the planar surface is calculated with a LoS distance of 5 m. For each different standard deviation value, the simulation program is run five times. Averages of these simulations are calculated and the final results are presented in Figure 3.6. RMS error has small variations the until noise level equals 0.8 units. After this level, RMS sharply increases. For noise with standard deviation greater than 0.8 units, most of the noisy signal exceeds the threshold and gives erroneous estimation results. In real-time applications, first, standard deviation of noise can be estimated and then the transmitted signal amplitude and the threshold can be adjusted to decrease the RMS error.

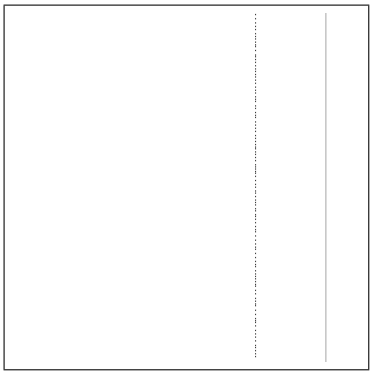

(a)

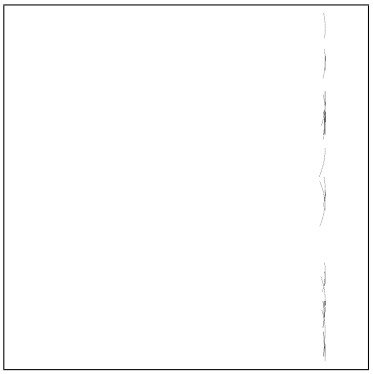

(b)

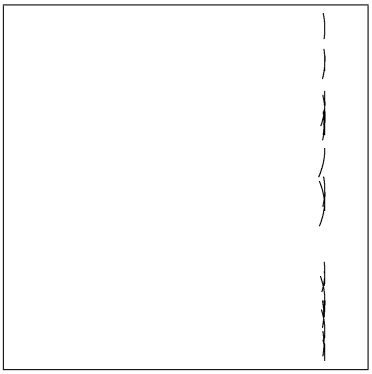

(c)

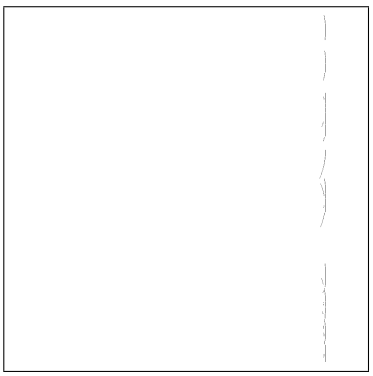

(d)

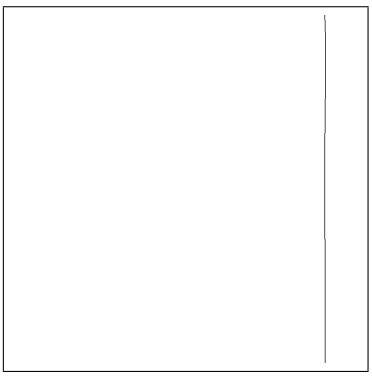

(e)

Figure 3.2: a) Actual surface profile and the transducers which are located 2 m away from the actual surface, b) estimated surface profile, c) the result of low-pass filtering, d) the result of thinning, and e) polynomial fit of order 5. E_{rms}=0.72 cm.

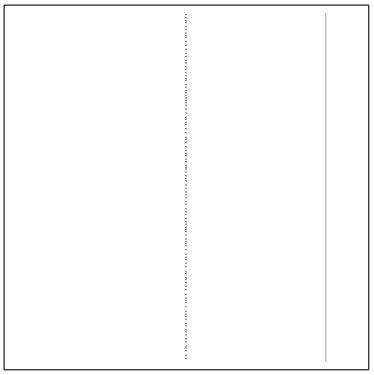

(a)

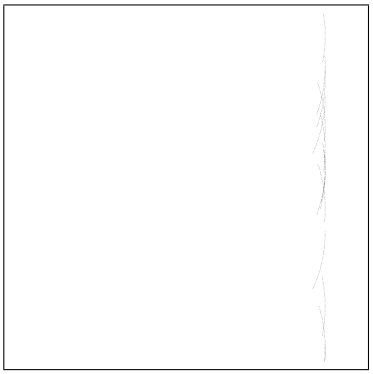

(b)

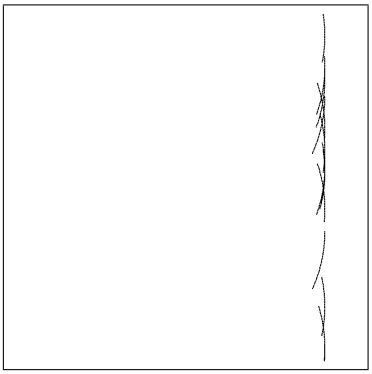

(c)

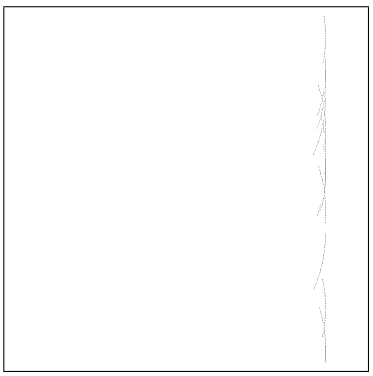

(d)

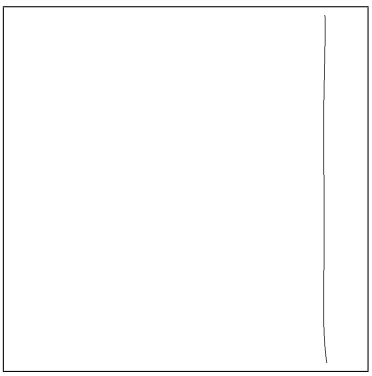

(e)

Figure 3.3: a) Actual surface profile and the transducers which are located 4 m away from the actual surface, b) estimated surface profile, c) the result of low-pass filtering d) the result of thinning, and e) polynomial fit of order 5. E_{rms}=3.14 cm.

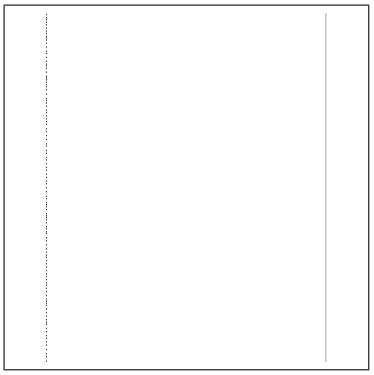

(a)

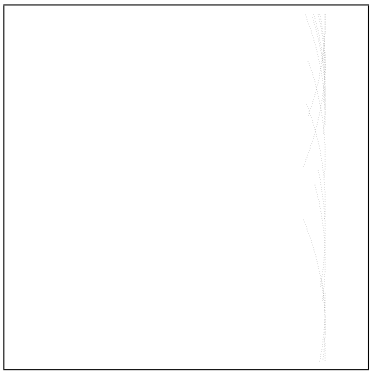

(b)

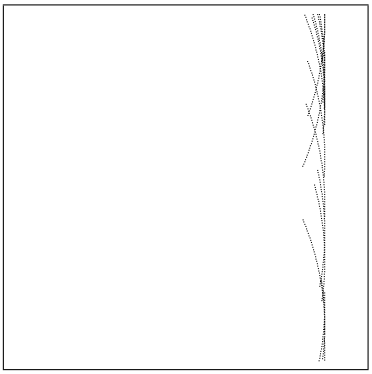

(c)

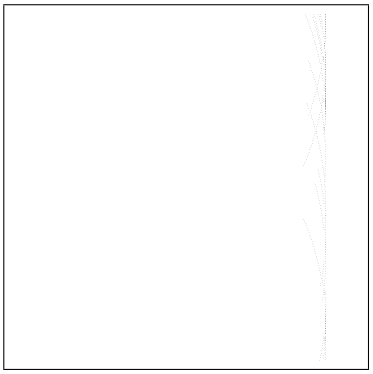

(d)

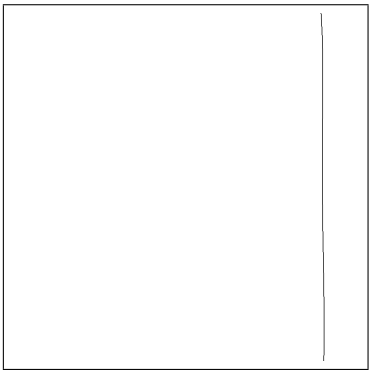

(e)

Figure 3.4: a) Actual surface profile and the transducers which are located 8 m away from the actual surface, b) estimated surface profile, c) the result of low-pass filtering, d) the result of thinning, and e) polynomial fit of order 5. E_{rms}=6.69 cm.

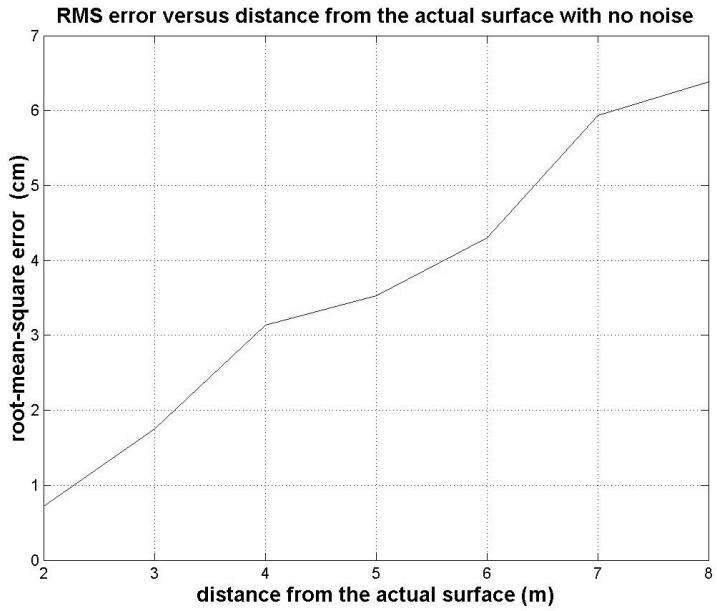

Figure 3.5: RMS error for the planar surface profile estimation with no noise.

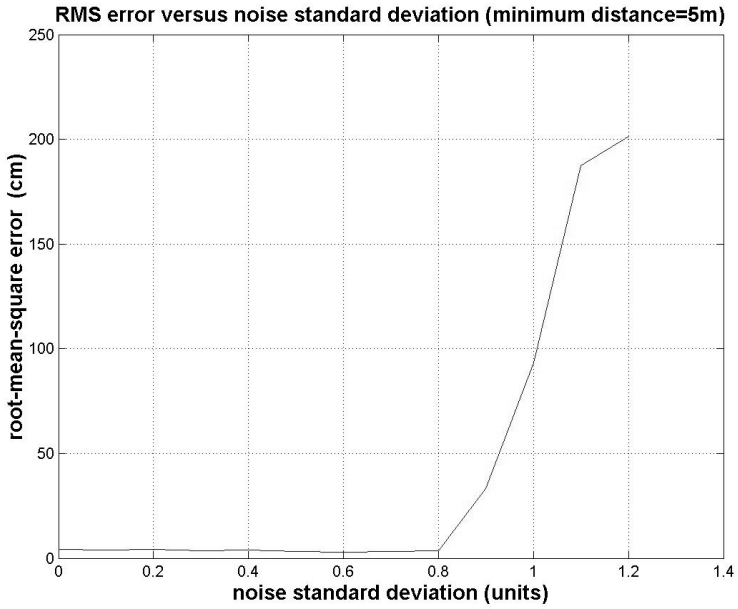

Figure 3.6: RMS error versus standard deviation of noise for the planar surface at 5 m.

3.2 Results for the Corner

For the second simulation, the program is re-run for the corner. In the first run, short separation for transducers and actual surface distance is taken as 4 m. Actual surface profile and transducers are shown in Figure 3.7(a). After scanning the environment, and estimated surface profile is extracted (Figure 3.7(b)). There are some gaps on the surface curvature of the estimated map. Spatial low-pass filtering process is applied on the estimation map to fill these gaps. Then, thinning process is applied to have the final estimation map which is shown in Figure 3.7(b).

In the second run, simulation is done for medium distances. Figure 3.8(a) shows the localization of transducers which are located away from the vertex of the corner with a distance of 7 m. Estimated surface profile is given in Figure 3.8(b). Again, some gaps occur on the curvature of the estimated profile. Result of low-pass filtering is presented in Figure 3.8(c). Final process is thinning and the result of this process is given in Figure 3.8(d).

At the final run for the simulation of the corner, program is run for far distance of transducer and actual surface separation. Figure 3.9(a) shows the localization of the transducers which are located away from actual surface with a distance of 9 m. Estimated surface profile is given in Figure 3.9(b). Results of low-pass filtering and thinning is given in Figure 3.9(c) and 3.9(d).

The simulation results show that the number of gaps on the estimated surface profile increases as the transducers are localized further away from the actual surface. RMS error for the corner is directly proportional to the distance between the transducer array and corner. Corner profile can be extracted from the estimation map up to 9 m separation of the transducers and vertex of the corner.

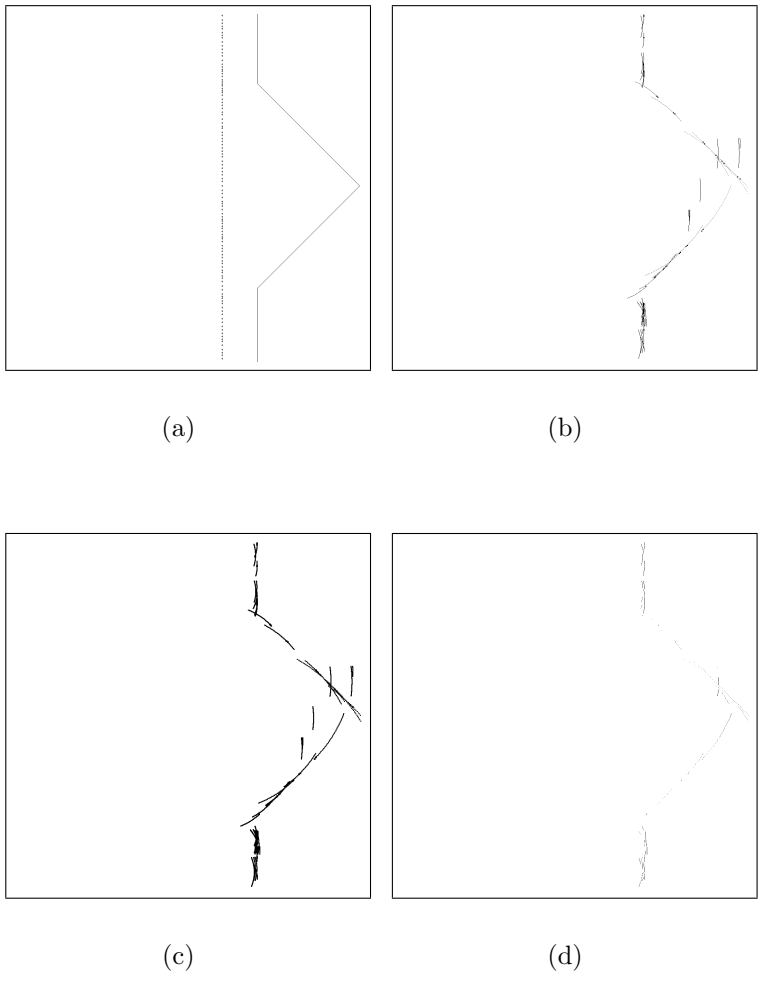

Figure 3.7: a) Actual surface profile and the transducers which are located 4 m away from the vertex of the corner, b) estimated surface profile, c) the result of low-pass filtering, and d) the result of thinning.

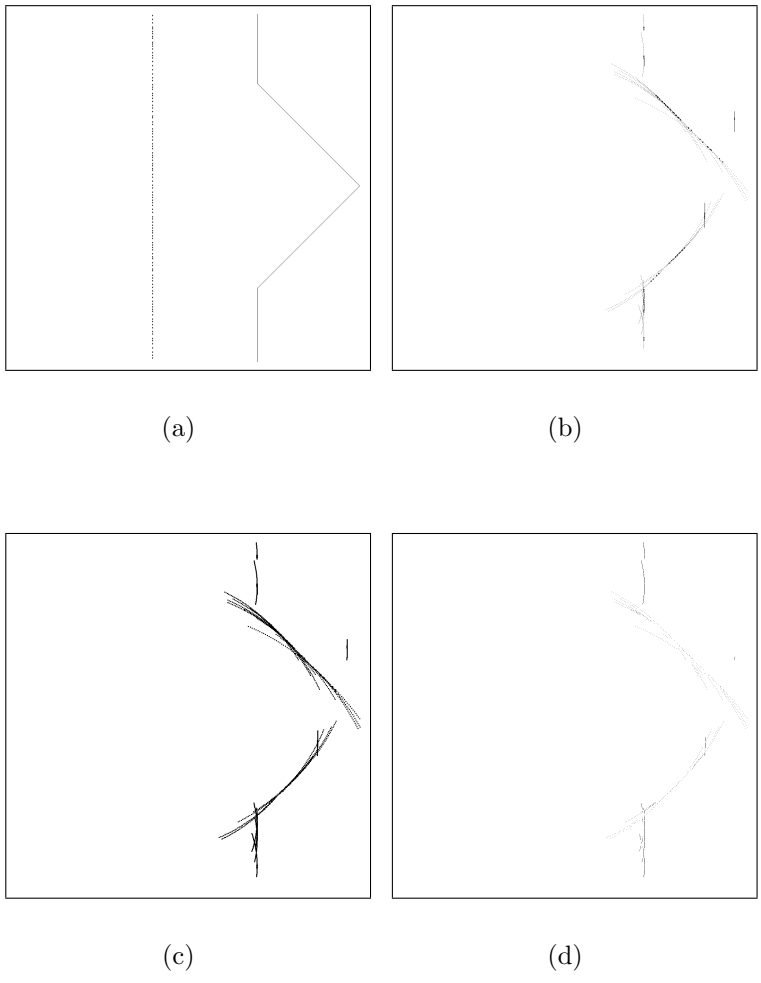

(a) (b)

(c) (d)

Figure 3.8: a) Actual surface profile and the transducers which are located 7 m away from the vertex of the corner, b) estimated surface profile, c) the result of low-pass filtering, and d) the result of thinning.

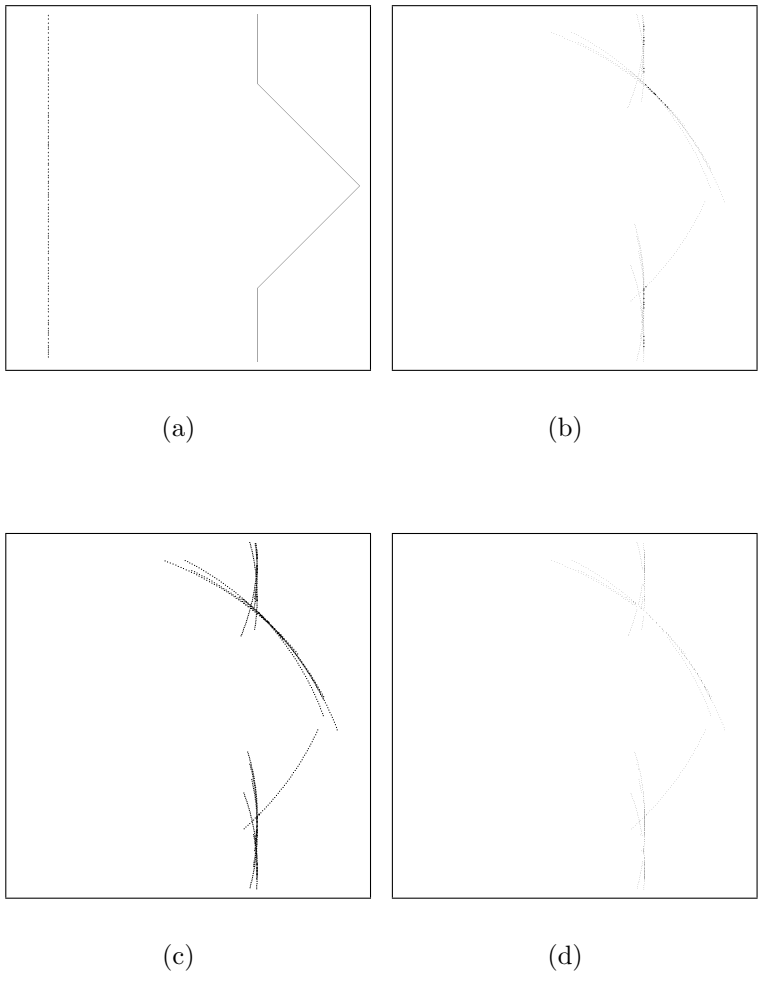

Figure 3.9: a) Actual surface profile and the transducers which are located 9 m away from the vertex of the corner, b) estimated surface profile, c) the result of low-pass filtering, and d) the result of thinning.

3.3 Results for the Edge

Simulations are performed for the edge target type. Results of scanning process are presented in Figures 3.10–3.12. In the first run, array elements are localized 1 m away from the vertex of the edge for short distance of array and surface separation. The estimated surface profile is presented in Figure 3.10(b). There are a lot of gaps on the estimated surface curvature. Low-pass filter is applied on the two dimensional occupancy map and the result is shown in Figure 3.10(c). After this process, some redundant arcs occur on the estimation map. Thinning process is applied on the filtered estimated map (Figure 3.10(d)).

In the second run, array elements are 3 m away from the vertex of the edge (Figure 3.11(a)). Estimated surface profile is shown in Figure 3.11(b). Results of low-pass filtering and thinning are presented in Figures 3.11(c) and 3.11(d).

In the final simulation, array distance from the vertex of the edge is taken as 5 m (Figure 3.12(a)). Estimated surface profile is given in Figure 3.12(b). Results of filtering and thinning are shown in Figures 3.12(c) and 3.12(d). In this run, one of the walls of the edge and vertex of the edge cannot be extracted from the estimated map.

Simulation results for the edge show that the method works up to 3-4 m separation of the transducers and vertex of the edge. As the array goes away from the vertex of edge accuracy of estimation map decreases and RMS error increases. As the array distance increases, RMS error also increases.

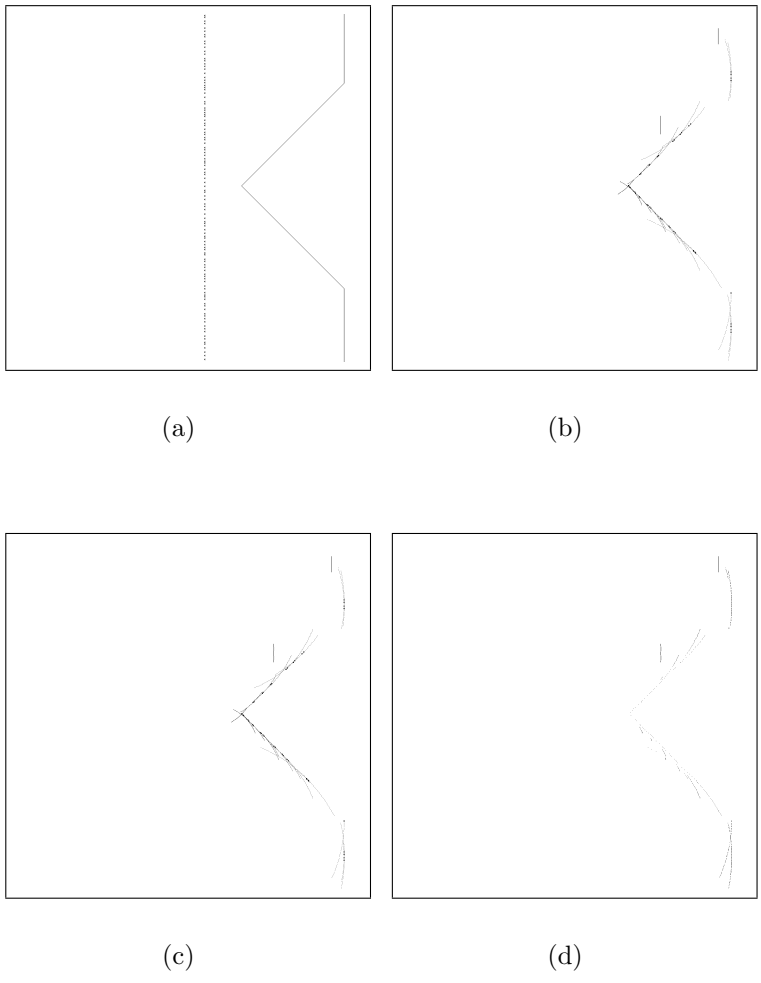

(a) (b)

(c) (d)

Figure 3.10: a) Actual surface profile and the transducers which are located 1 m away from the vertex of the edge, b) estimated surface profile, c) the result of low-pass filtering, and d) the result of thinning.

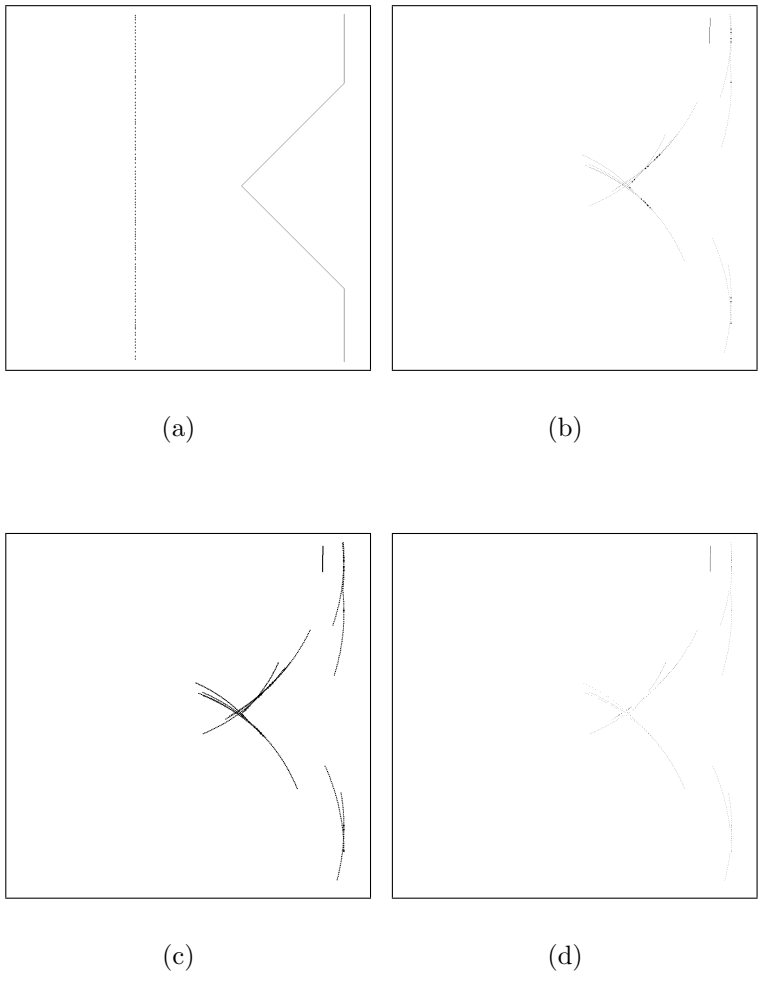

Figure 3.11: a) Actual surface profile and the transducers which are located 3 m away from the vertex of the edge, b) estimated surface profile, c) the result of low-pass filtering, and d) the result of thinning.

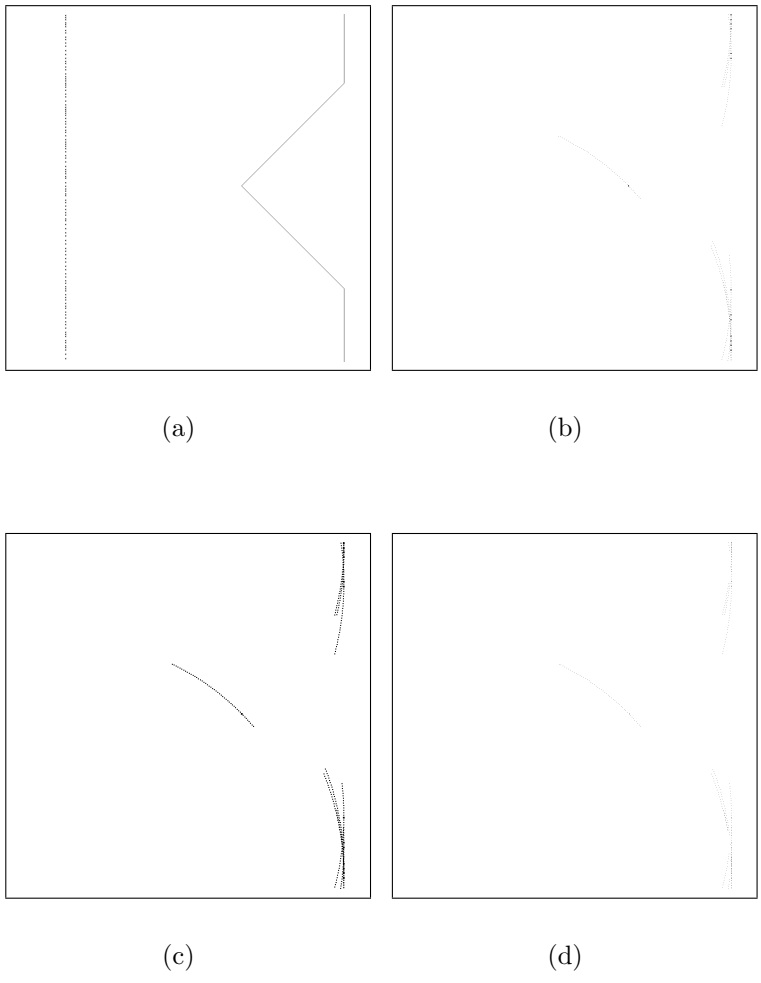

(a) (b)

(c) (d)

Figure 3.12: a) Actual surface profile and the transducers which are located 5 m away from the vertex of the edge, b) estimated surface profile, c) the result of low-pass filtering, and d) the result of thinning.

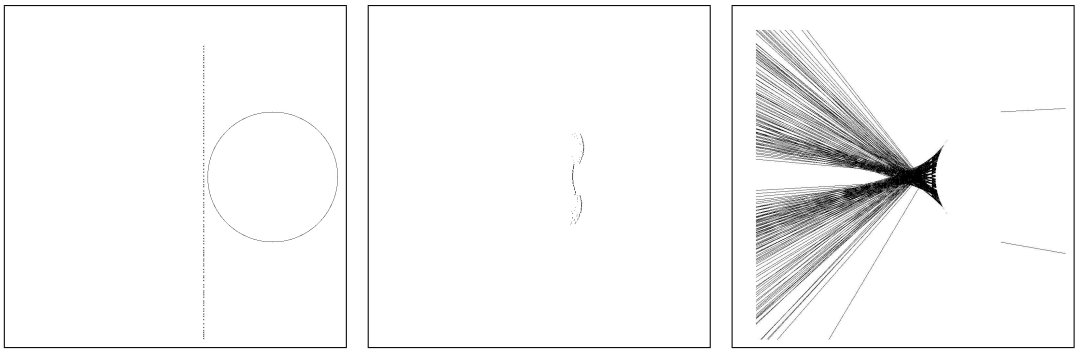

(a) (b) (c)

Figure 3.13: a) Actual surface profile and the transducers which are located 2.1 m away from center of the cylinder of radius 2 m, b) estimated surface profile, and c) echo distribution directions.

3.4 Results for the Cylinder

In the cylinder simulation model, a cylinder with radius 2 m is located near one of the walls of a 10mx10m area. The same localization procedure is used for the transducers. Cylinder type surfaces reflect the echo to the transducers while they are located within the sensitivity region of transducers. In the simulation process, most of the echoes cannot be detected by the transducers. Simulation results are presented in Figures 3.13-3.15. In the first run, array elements are located 2.1 m away from the center of the cylinder. Only transducers whose LoS region cross over the center of the cylinder can detect the surface. The transmitted signal hits the cylinder and the reflected signals produce on the radiation patterns shown in Figures 3.13(c), 3.14(c), and 3.15(c). In the radiation pattern, most of the signals go outside the sensitivity region. The distance between the array elements and the origin of the cylinder is taken as 3 m and the results are shown in Figure 3.14. In the final run, array elements are located 4 m away from the center of the cylinder. Results are presented in Figure 3.15. As the distance between array elements and the center of the cylinder decreases, estimated surface length increases. Simulation results are not sufficient for extracting the cylinder surface profile completely as a closed curve. Since the beamwidth of the transducer is so narrow, LoS located cylinder type objects can be detected by ultrasonic sensors.

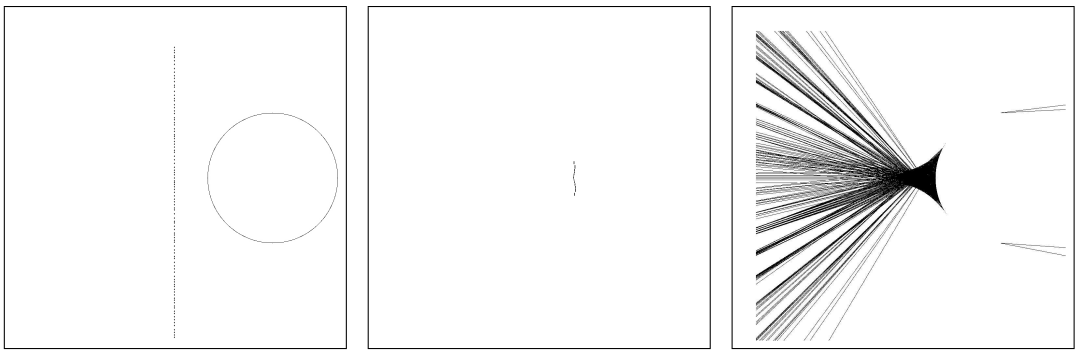

(a) (b) (c)

Figure 3.14: a) Actual surface profile and the transducers which are located 3 m away from center of the cylinder of radius 2 m, b) estimated surface profile, and c) echo distribution directions.

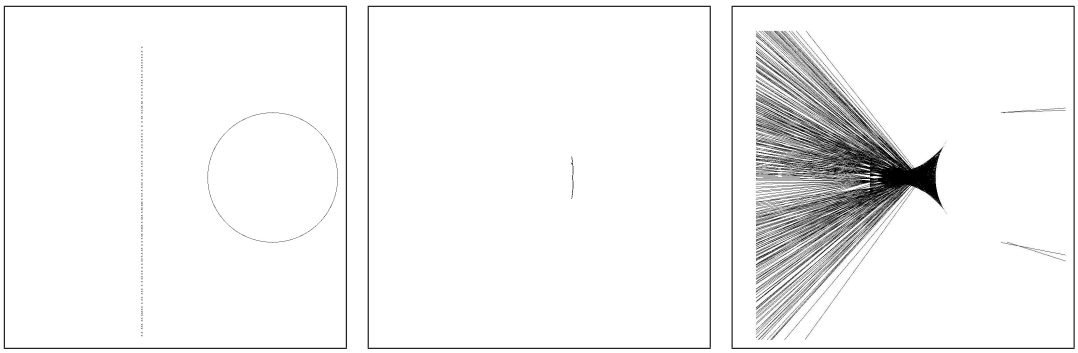

(a) (b) (c)

Figure 3.15: a) Actual surface profile and the transducers which are located 4 m away from center of the cylinder of radius 2 m, b) estimated surface profile, and c) echo distribution directions.

3.5 Results for the Sinusoidal Surface

In sinusoidal surface profile simulation, one element of the transducer array is randomly located in the environment. Other elements of the array are located away from the first element. Separations between the centers of the elements of the array varies between 5 to 12 cm. Localization of the array elements continues until total localized array length reaches 10 m. In the first run, array elements are localized 1 m away from the shortest LoS distance from the sinusoidal surface profile (Figure 3.16(a)). The actual sinusoidal surface profile and the array configuration are presented in Figure 3.16(a). Simulation result without filtering is shown in Figure 3.16(b). As a next step, a spatial low-pass-filter (LPF) is applied on the estimated surface profile. After this result, some of the un-scanned surface profile is estimated (Figure 3.16(c)). This procedure also increases redundant arcs. Thinning process is applied for clearing redundant arcs (Figure 3.16(d)). A polynomial fitting procedure is applied for finalizing the surface profile estimation. (Figure 3.16(e)). RMS error for the first run is 13.72 cm. After the first run, simulation is re-run for the conditions in which array elements are localized 4 m away from the surface of the planar wall (Figure 3.17(a)). Results of the simulation stages 1-4 are illustrated in Figure 3.17(b). This result is convolved with a LPF and then, thinning procedure is applied (Figure 3.17(c)-3.17(d)). Final estimation result with polynomial fit of order 7 is displayed in Figure 3.17(e) with an RMS error 16.55 cm. Third run results are represented in Figure 3.18(a)-3.18(e). RMS error is also calculated for sinusoidal surface profile in Figure 3.19. RMS error increases as the distance between the array elements and the actual surface increases. Simulations are also done for additive noise with varying standard deviation levels. For each noise level, averages of five runs are calculated for a minimum array size and actual surface distance of 5 m. Results of varying noise levels are shown in Figure 3.20.

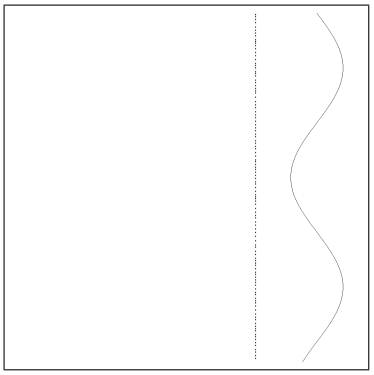

(a)

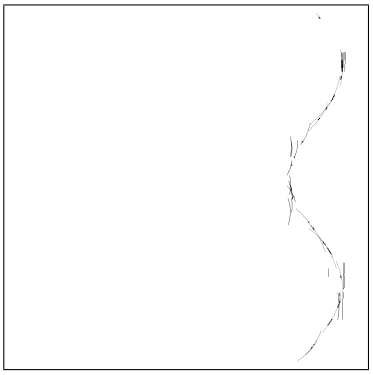

(b)

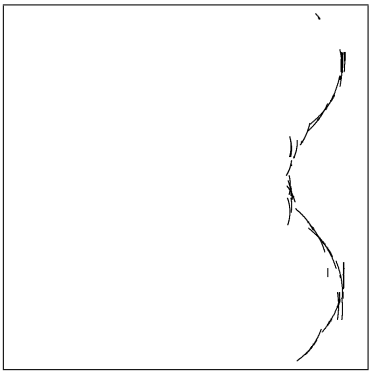

(c)

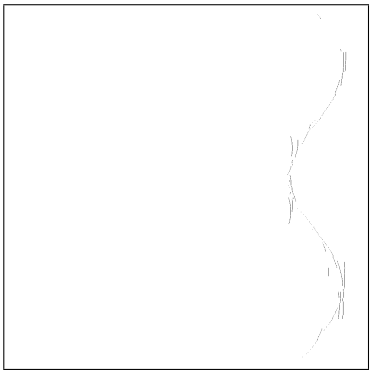

(d)

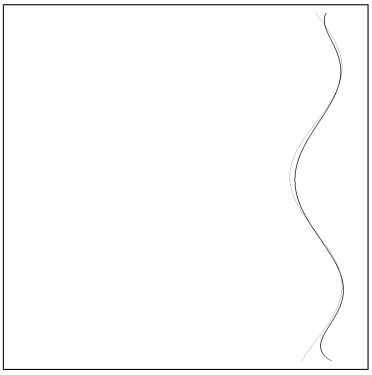

(e)

Figure 3.16: a) Actual surface profile and the transducers located 1 m away from the actual surface, b) estimated surface profile, c) the result of low-pass filtering, d) the result of thinning, and e) polynomial fit of order 8. E_{rms}=13.72 cm.

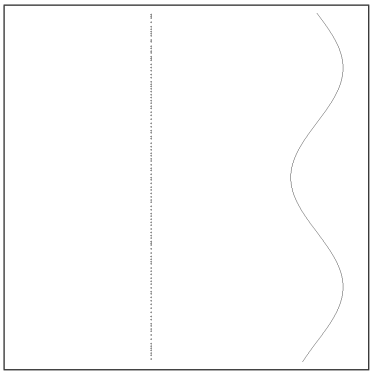

(a)

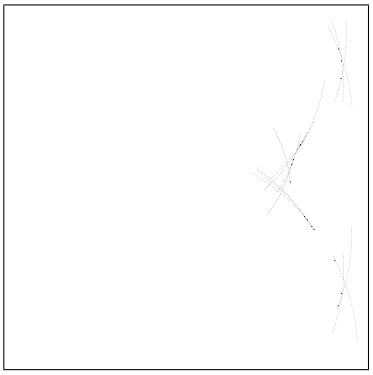

(b)

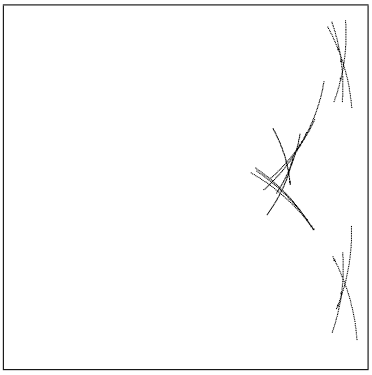

(c)

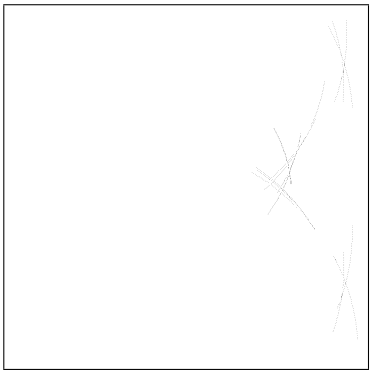

(d)

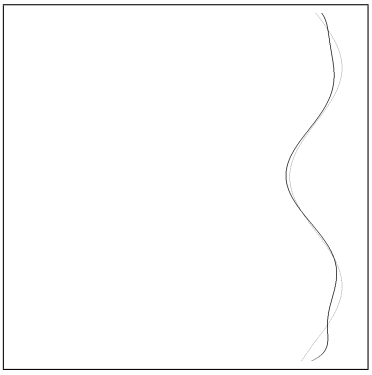

(e)

Figure 3.17: a) Actual surface profile and the transducers located 4 m away from the actual surface, b) estimated surface profile, c) the result of low-pass filtering, d) the result of thinning, and e) polynomial fit of order 8. E_{rms}= 16.54 cm.

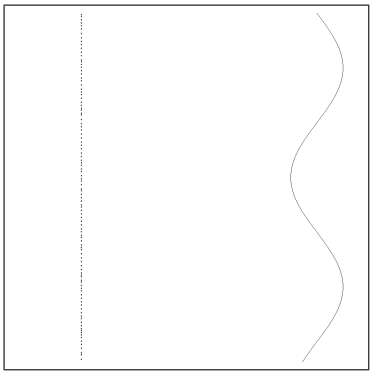

(a)

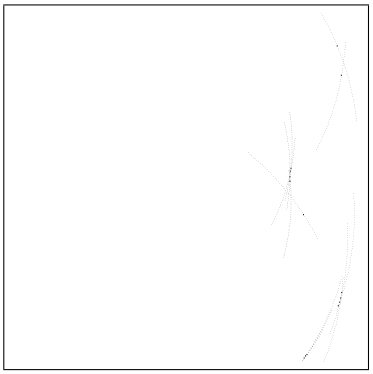

(b)

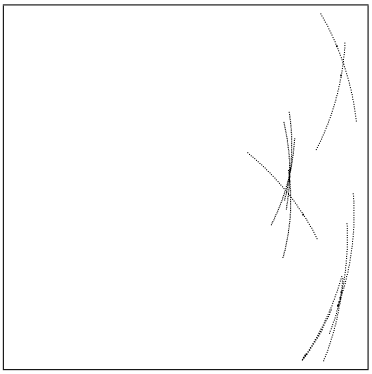

(c)

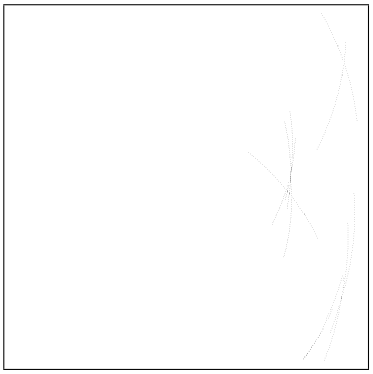

(d)

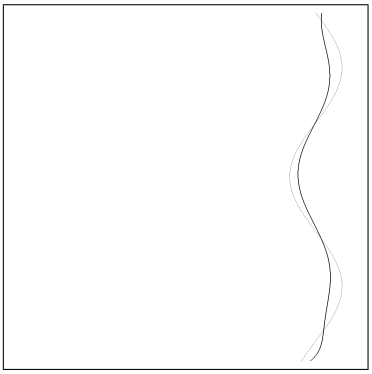

(e)

Figure 3.18: a) Actual surface profile and the transducers located 6 m away from the actual surface, b) estimated surface profile, c) the result of low-pass filtering, d) the result of thinning, and e) polynomial fit of order 8. E_{rms}= 22.80 cm.

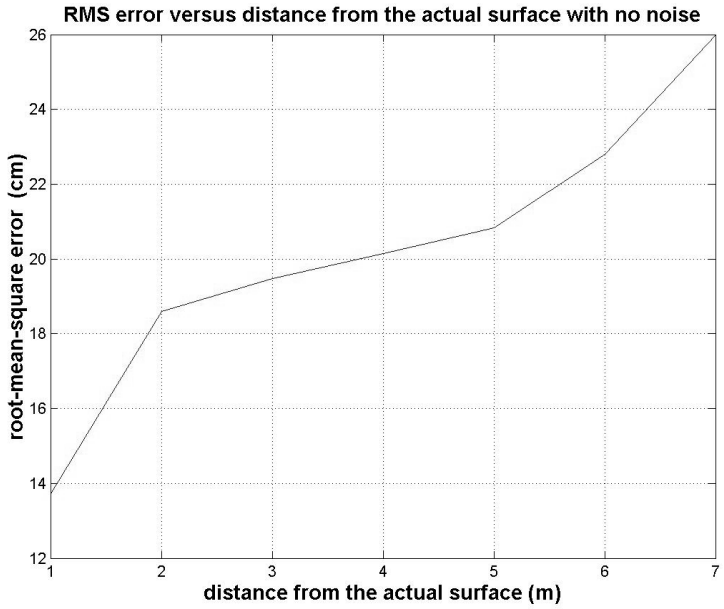

Figure 3.19: RMS error for the sinusoidal surface profile estimation with no noise.

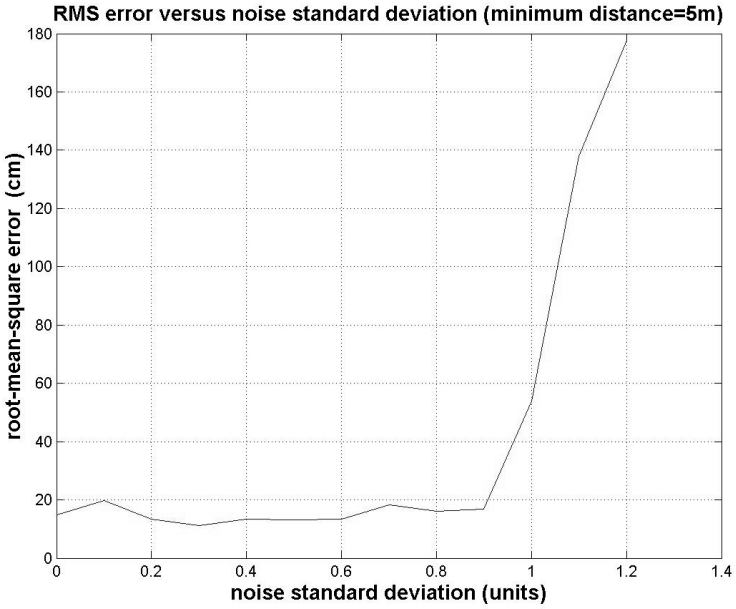

Figure 3.20: RMS error versus standard deviation of noise for the sinusoidal surface profile estimation.

3.6 Results for the Closed Environment

Finally, closed environments composed of walls, corners, edges, and cylinders are modelled. In the room, each wall is scanned independently. In the first model, a transducer array with 10 elements is used. Transducers are localized as in the previous simulations for each of the scanned walls of the room. The normal of the transducer array is turned by 90° after each wall scan. Actual room surface is given in Figure 3.21(a), and the localization of the transducers is shown in Figure 3.21(b). Simulation results of each wall are combined and the extracted map of the environment is displayed in Figure 3.21(c). Some gaps occur in the constructed map. Positions of the array elements are changed. Transducer elements are localized along the same line with different separations but after one scan, LoS distance is changed. Positions of the array elements are shown in Figure 3.22(b). The scanning result is displayed in Figure 3.22(c). This process gives better estimated map but it is not very good at the vertex of the edges and corners.

An extended simulation model may be used for improved estimation which is given in Chapter 2. An extended algorithm is used for scanning the closed room model. A circular transducer array is used for the simulations. The center of the circular array is shifted by the step size in the environment. The resulting transducer map is illustrated in Figure 3.23(b), 3.24(b) and 3.25(b).

In the program, the step size can vary from 25 to 150 cm. The actual surface profile, transducer locations, and estimated surface profiles are shown in Figure 3.23(b) and 3.23(c). In the first simulation, the step size is taken as 50 cm. Localization of the array elements in the environment is presented in Figure 3.23(b). The estimated surface profile is shown in Figure 3.23(c). In the estimated map, all of the simulated surfaces are accurately estimated. In Figure 3.24, simulation is worked with step size 70 cm. The estimated surface profile is shown in Figure 3.24(c). In the estimated surface profile, one of the edges (left-bottom) cannot be estimated accurately. Planar surfaces and vertex of corners are accurately estimated. A simulation result with step size 75 cm is presented in Figure 3.24. Circular-array elements are localized as in Figure 3.24(b). The

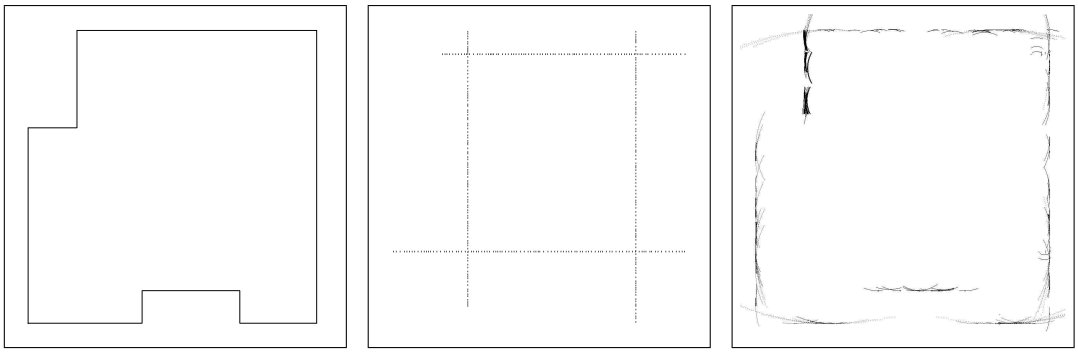

(a) (b) (c)

Figure 3.21: a) Actual surface profile, b) transducer array positions, and c) estimated surface profile.

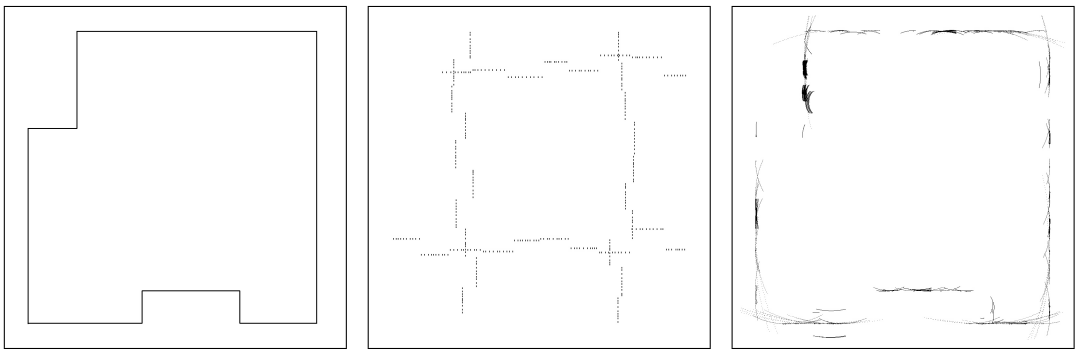

(a) (b) (c)

Figure 3.22: a) Actual surface profile, b) transducer array positions, and c) estimated surface profile.

estimated surface profile is presented in Figure 3.24(c). Again, vertex estimation problem occurs. As the step size increases, un-scanned parts of the environment increase so corners and edges cannot be estimated realistically. In a closed room, a simulation step size of 50 cm is sufficient to estimate any type of surface profile.

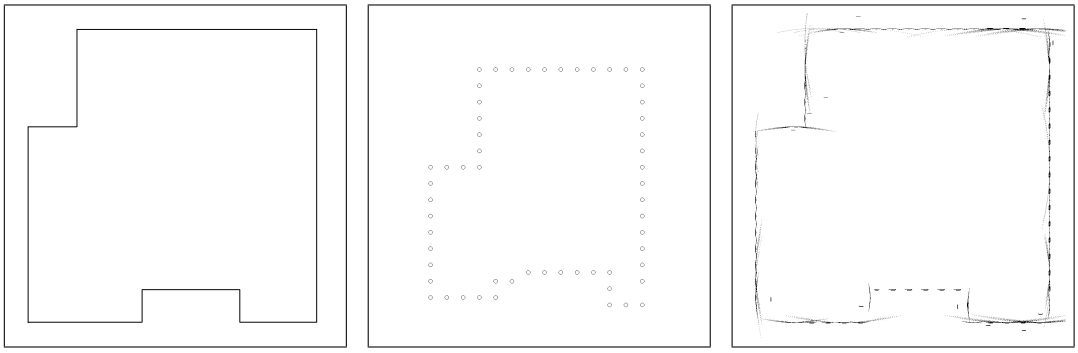

(a) (b) (c)

Figure 3.23: a) Actual surface profile, b) circular transducer array locations, and c) estimated surface profile with step size=50 cm.

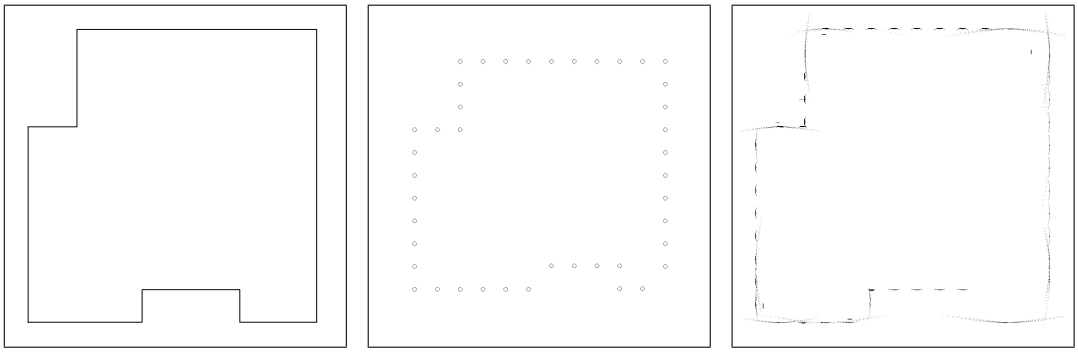

(a) (b) (c)

Figure 3.24: a) Actual surface profile, b) circular transducer array locations, and c) estimated surface profile with step size=70 cm.

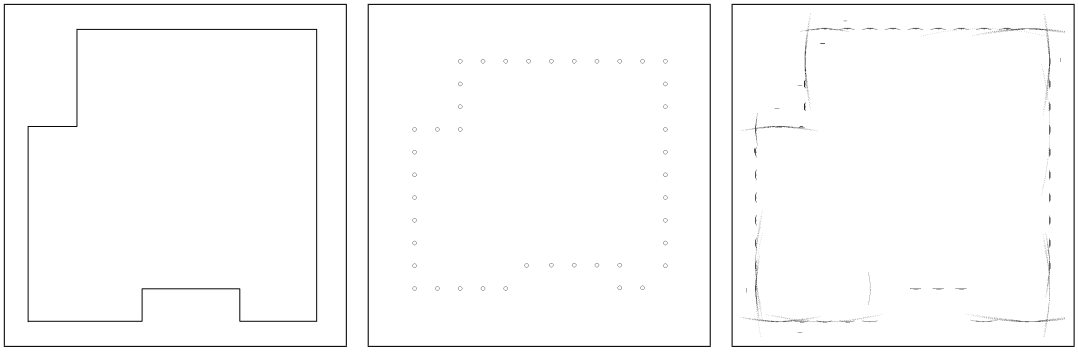

(a) (b) (c)

Figure 3.25: a) Actual surface profile, b) circular transducer array locations, and c) estimated surface profile with step size=75 cm.

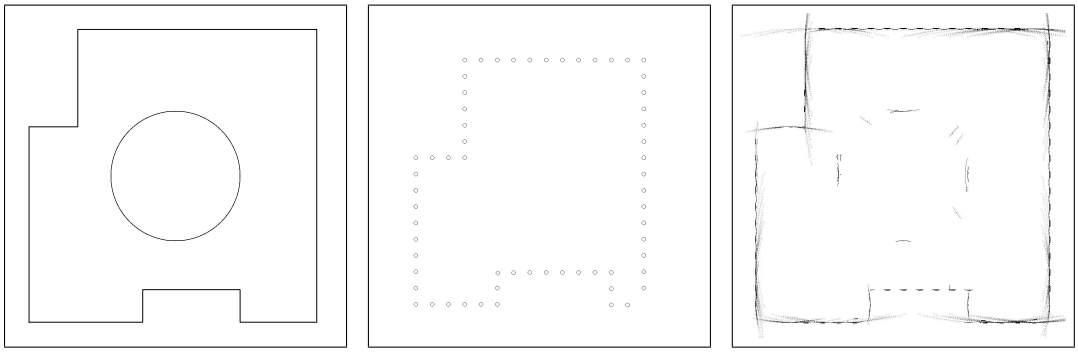

(a) (b) (c)

Figure 3.26: a) Actual surface profile. A cylinder with radius of 2 m is located at center of the environment, b) circular transducer array locations, and c) estimated surface profile with step size=50 cm.

In another simulation, a cylinder with radius 2 m is located at the center of the room (Figure 3.26(a)). The wall-following algorithm is applied for the localization of the circular transducer array (Figure 3.26(b)). The simulation result is presented in Figure 3.26(c). Planar walls, edges, and corners can be easily extracted from the estimated map. Some of the boundaries of the cylinder can be extracted. In the cylinder model, most of the echoes are distributed outside of the joint sensitivity region of the transducer elements so that only those transducers whose LoS regions overlap with the cylinder can detect the surface of the cylinder.

3.7 Computational Cost

The algorithm works best with random localization and orientation of the transducers. Computation time of the algorithm depends on transducers localization, orientation, and surface profile. Most of the computation time is spent for matrix and file operations. Multiple reflections and strictly varying surface profiles increases computation time. The algorithm can extract surface profiles of planar

surfaces and cylinders very fast. The computation time varies between 8-20 seconds depending on the distance between the transducers and the actual surface profile. In the cylinder model, echoes are rarely received by the transducers. Since the number of received echo signals is less than the ones for the plane, map building time for the cylinder is less than the time spent for a plane. In the cylinder model, most of the time is spent for calculating the echo reflection directions. In real-time applications, the waveform can be recorded within a few microseconds and with a few calculations, and the surface profile can be extracted with high accuracy. Computation time for the corner and the edge is a few seconds longer than the plane. Multiple-reflections occur, but most of these reflections stay below the threshold and these reflections are ignored in the map drawing stages of the simulation. Profiles of sinusoidal type surfaces can be extracted with high accuracy within 15-30 seconds. In the simulation process, multiple-reflections for the sinusoidal surfaces stay over the threshold and this increases the computation time by a few seconds depending on the orientation and localization of the transducers. In the simulation of closed environments, algorithm is extended to extract high resolution maps. Computation time increases up to 2 minutes depending on the localization of the circular array. In this model, the time required for moving the circular transducer array is ignored. In real-time applications, computation time increases by a few minutes depending on the velocity of the carrier unit of the circular transducer array. The method is computation-wise, cheap and suitable for extracting surface profiles of indoor environments.

Chapter 4

Conclusions and Future Work

In this work, a simulation model for extracting profiles of indoor environments is developed. The method is suitable for plane, corner, edge, cylinder, and sinusoidal surfaces as well as indoor environments made of these basic target types. Planes, corners and sinusoidal type objects can be extracted from the estimation map up to 9 m separation of transducers and actual surface. Edges can be extracted up to 4 m separation. For cylinder model, surface curvature of the cylinder can be extracted only for the regions which are within the joint sensitivity region of the transducers. Some problems occur for the detection of surfaces with sharp corners and edges where the curvature changes abruptly. When the wall-following algorithm is employed, these problems are remedied. Since the circularly localized array has 360° point of view, closed environments can be scanned with higher resolution. Circularly configured array can extract the map very fast so that this model can be used in real-time scanning of indoor environments. The method can extract basic object profiles in less than 30 seconds. For closed room models, simulation result is taken in two minutes. In real-time applications, the waveform can be recorded within a few microseconds and with a few calculations, and the surface profile can be extracted with high accuracy. The method is usable for industrial applications such as car parking systems, equipment and product carrier units in factories. Car parking systems can be redesigned with cheaper sensors producing a more accurate environment map. Equipment carrier units

can extract factory maps within a few minutes, and all the carriage applications can be done faster and more safely. As for future work, the simulation model will be improved to decrease the RMS error for edge and cylinder surfaces. The simulation results can be compared with real data and better models can be developed. Another direction for future research is extending the method to include other sensing modalities such as infrared and laser.

Bibliography

[1] A. Elfes. Sonar-based real-world mapping and navigation. *IEEE Journal of Robotics and Automation*, 3(3):249–265, 1987.

[2] A. J. Cetto and A. Sanfeliu. Learning of dynamic environment by a mobile robot from stereo cues. *International Conference on Multisensor Fusion and Intelligent Systems*, pages 305–310, August 2001.

[3] A. J. Cetto and A. Sanfeliu. Concurrent map building and localization with landmark validation. *International Conference on Pattern Recognition*, II(16):693–696, August 2002.

[4] B. Schiele and J. L. Crowley. Comparison of position estimation techniques using occupancy grids. *Proceedings of IEEE International Conference on Robotics and Automation*, San Diego, California:1459–1467, May 1994.

[5] C. Jennings, D. Murray and J. J. Little. Cooperative robot localization with vision-based mapping. *Proceedings of IEEE International Conference on Robotics and Automation*, Detroit, Michigan:2659–2665, May 1999.

[6] D. Başkent and B. Barshan. Surface profile determination from multiple sonar data using morphological processing. *International Journal of Robotics Research*, 18(8):788–808, August 1999.

[7] D. Başkent and B. Barshan. Morphological surface profile extraction with multiple range sensors. *Pattern Recognition*, 34:1459–1467, 2001.

[8] D. Murray and C. Jennings. Stereo vision based mapping and navigation for mobile robots. *Proceedings of IEEE International Conference on Robotics and Automation*, New Mexico, USA:20–25, April 1997.

[9] D. Novick, C. Crane and D. Armstrong. Implementation of a sensor fusion-based obstacle-detection component for an autonomous outdoor vehicle. *Proceedings of the 2002 Florida Conference on Recent Advances in Robotics*, Miami, USA, May 2002.

[10] F. H. Wullschleger, K. O. Arras and S. J. Vestli. A flexible exploration framework for map building. *Proceedings of the Third European Workshop on Advanced Mobile Robots (Eurobot 99)*, Zurich, Switzerland:49–57, September 1999.

[11] F. Sempé. Autonomous mobile robotics: Localization and navigation with a region based map. *14th European Conference on Artificial Intelligence (ECAI 2000)*, 2000.

[12] H. Baltzakis and P. Trahanias. An iterative approach for building feature maps in cyclic environments. *Proceedings of the IEEE/RSJ International Conference on Intelligent Robots and Systems*, pages 576–581, October 2002.

[13] H. Hu and D. Gu. Landmark-based navigation of autonomous robots in industry. *International Journal of Industrial Robot*, 27(6):458–467, November 2000.

[14] H. J. Jeon and B. K. Kim. Feature-based probabilistic map building using time and amplitude information of sonar in indoor environments. *Robotica*, 19:423–437, 2001.

[15] J. A. Castellanos, J. Neira and J. D. Tardos. Multisensor fusion for simultaneous localization and map building. *IEEE Transactions on Robotics and Automation*, 17(6):908–914, December 2001.

[16] J. Borenstein and Y. Koren. Histogramic in-motion mapping for mobile robot obstacle avoidance. *IEEE Journal of Robotics and Automation*, 7(4):535–539, 1991.

[17] J. Guivant and E. Nebot. Solving computational and memory requirements of feature based simultaneous localization and map building algorithms. *Tech. rep., Australian Center for Field Robotics, University of Sydney*, 2002.

[18] J. Guivant, E. Nebot and S. Baiker. Autonomous navigation ad map building using laser range sensors in outdoor applications. *Journal of Robotic Systems*, 17(10):565–583, October 2000.

[19] K. O. Arras, J. A. Castellanos, M. Schilt and R. Siegwart. Feature extraction and scene interpretation for map-based navigation and map building. *Proceedings of SPIE, Mobile Robotics XII*, 3210:42–53, 1997.

[20] K. O. Arras, J. A. Castellanos, M. Schilt and R. Siegwart. Towards feature-based multi-hypothesis localization and tracking. *4th European Workshop on Advanced Mobile Robots (Eurobot'01), Lund, Sweden*, pages 57–65, September 2001.

[21] M. Betke and L. Gurvits. Mobile robot localization using landmarks. *IEEE Transactions on Robotics and Automation*, 13(2):251–263, April 1997.

[22] M. Caccia, G. Bruzzone and G. Veruggio. Active pan-tilt bi-unit sonar head: Design and preliminary rules. *Massimo Caccia, project of PRASSI*, 2002.

[23] M. Jun and R. Andrea. Probability map building of uncertain dynamic environments with indistinguishable obstacles. *Proceedings of the American Control Conference*, Denver, Colorado, June 2003.

[24] M. Kam, X. Zhu and P. Kalata. Sensor fusion for mobile robot navigation. *Proceedings of the IEEE*, 85(1):108–119, January 1997.

[25] M. W. M. G. Dissanayake, P. Newman, S. Clark, H. F. Durrant-Whyte and M. Csorba. A solution to the simultaneous localization and map building (slam) problem. *IEEE Transactions on Robotics and Automation*, 17(3):229–241, June 2001.

[26] P. Jensfelt, D. J. Austin, O. Wijk and M. Andersson. Feature based condensation for mobile robot localization. *Proceedings of IEEE International Conference on Robotics and Automation*, pages 2531–2537, April 2000.

[27] P. Newman, M. Bosse and J. Leonard. Autonomous feature-based exploration. *Proceedings of IEEE International Conference on Robotics and Automation*, Taipei, Taiwan, 2003.

[28] R. C. Gonzales and R. E. Woods. Digital image processing. *Addison-Wesley*, page Chapters 4 and 8, 1993.

[29] R. Kuc and M.W. Siegel. Physically based simulation model for acoustic sensor robot navigation. *IEEE Transactions on Pattern Analysis and Machine Intelligence*, pages 766–788, November 1987.

[30] V. Varveropoulos. Robot localization and map construction using sonar data. *The rossum project,http://rossum.sourceforge.net*, April 2002.

[31] Z. Yi H. Y. Khing, C. C. Seng and Z. X. Wei. Multi-ultrasonic sensor fusion for mobile robots. *First IEEE Workshop on Sensor Network Protocols and Applications (SNPA 2003)*, May 2003.